SUPPLEMENTAL MATERIAL

Anti-Inflammatory and Cytotoxic Agents from *Xylaria* sp. SWUF09-62 Fungus

Theerawat Patjana [a], Phongphan Jantaharn [a], Praewpan Katrun [a], Wiyada Mongkolthanaruk [b], Nuttika Suwannasai [c], Thanaset Senawong [d], Sarawut Tontapha [e], Vittaya Amornkitbumrung [e,f], Sirirath McCloskey [a,*]

[a] *Natural Products Research Unit, Centre of Excellence for Innovation in Chemistry (PERCH-CIC), Department of Chemistry, Faculty of Science, Khon Kaen University, Khon Kaen 40002, Thailand.*

[b] *Department of Microbiology, Faculty of Science, Khon Kaen University, Khon Kaen 40002, Thailand.*

[c] *Department of Biology, Faculty of science, Srinakharinwirot University, Bangkok 10110, Thailand.*

[d] *Department of Biochemistry, Faculty of Science, Khon Kaen University, Khon Kaen 40002, Thailand.*

[e] *Department of Physics, Faculty of Science, Khon Kaen University, Khon Kaen 40002, Thailand.*

[f] *Institute of Nanomaterials Research and Innovation for Energy, Khon Kaen University, Khon Kaen 40002, Thailand.*

ABSTRACT

The ongoing search for anticancer agents from microorganisms led to the isolation of four new compounds including 6-ethyl-8-hydroxy-4*H*-chromen-4-one (**1**), 6-ethyl-7,8-dihydroxy-4*H*-chromen-4-one (**2**), (3*S*)-3,4-dihydro-8-hydroxy-7-methoxy-3-methylisocoumarin (**3**) and (3*S*)-3,4-dihydro-5,7,8-trihydroxy-3-methylisocoumarin (**4**), together with eleven known compounds (**5**-**15**) from *Xylaria* sp. SWUF09-62 fungus. The chemical structures were deduced from IR, 1D and 2D NMR, and MS data. The absolute configurations of **3** and **4** were determined by ECD experiment. Compounds **2** and **4** indicated possible chemoprevention and chemotherapeutic properties, exhibited anti-inflammatory properties by reducing nitric oxide production in LPS-stimulated RAW264.7 cells (IC_{50} = 1.57 ± 0.25 and 3.02 ± 0.27 μg/mL) and cytotoxicity against HT29 cells (IC_{50} = 16.46 ± 0.48 and 97.78 ± 7.14 μg/mL).

Keywords

Anti-inflammatory, Chromone, Cytotoxicity, Mellein, Nitric Oxide (NO), Xylaria

Contents

Lists of tables

Lists of figures

Experiment

General experimental procedures

All melting points were obtained using a Sanyo/Gallenkamp MPD350.BM3.5 melting point apparatus. Optical rotations were determined on the JASCO DIP-1000 digital polarimeter. The UV absorbance were measured on microplate reader (Bio-Rad laboratories, Hercules, CA). The CD spectra were recorded using a JASCO J-810 apparatus. IR spectra were determined on the Bruker TENSOR27 FT-IR spectrometer. The structural determination was based on the analysis of 1D (^{1}H and ^{13}C NMR) and 2D NMR (HMQC, HSQC, COSY, HMBC, and NOESY) spectral data, which were recorded on the Varian Mercury Plus 400 spectrometer. Column chromatography (CC) and flash column chromatography (FCC) were carried out using silica gel 60 (0.063-0.200 mm and 0.040-0.063 mm, Merck, Germany) and Sephadex LH-20 (Sigma-Aldrich, United States) for the molecule size separation. Preparative thin layer chromatography (PLC) was prepared using silica gel PF_{254} (Merck, Germany) as the stationary phase.

Computational details

Conformation analysis was carried out by Monte Carlo protocol through molecular mechanics force field using HyperChem software (HyperChem™ Professional 8.0.7, Hypercube, Inc., Gainesville, FL, USA), which resulted in one predominant molecular structure for both **3** and **4** for each conformer.. The geometrical optimizations of the resulting structures were reoptimized using the density functional theory (DFT) at the B3LYP level of theory and the 6-311G (d) basis set was used. For single point energy calculation, the transition energies used for generating the ECD spectra were computed with the time dependent density functional theory (TD-DFT) method using the long-range corrected functional CAM-B3LYP at the 6-311++G (d,p) level of theory (Yanai et al. 2004). The solvent effects were analyzed using the Conductor-like Polarizable Continuum Model (C-PCM) (Cossi et al. 2003). The calculations were performed using the GAUSSIAN 09 program (Frisch et al. 2010) and calculated ECD spectra were generated using the GaussSum program (Eko & Hiroshi 2014).

Table S1. The ^{1}H and ^{13}C NMR data of **1** (400 MHz, pyridine-d_5) and COSY and HMBC spectral data of **1**

Position		δ_H [a]	δ_C	**COSY**	**HMBC**
1					
2	CH	8.12 (d, 5.9)	156.0	3	3, 4, 8a
3	CH	6.47 (d, 5.9)	113.0	2	2, 4a
4			178.0		
4a			126.7		
5	CH	7.76 (d, 2.1)	113.8		4, 7, 8a, 9
6			142.2		
7	CH	7.37 (d, 2.1),	120.4		5, 8, 8a, 9
8			148.4		
8a			145.9		
9	CH_2	2.54 (q, 7.6)	29.0	10	5, 6, 7,10
10	CH_3	1.10 (t, 7.6)	15.9	9	6, 9

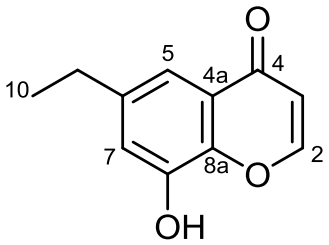

Figure S1. Structure of compound **1.**

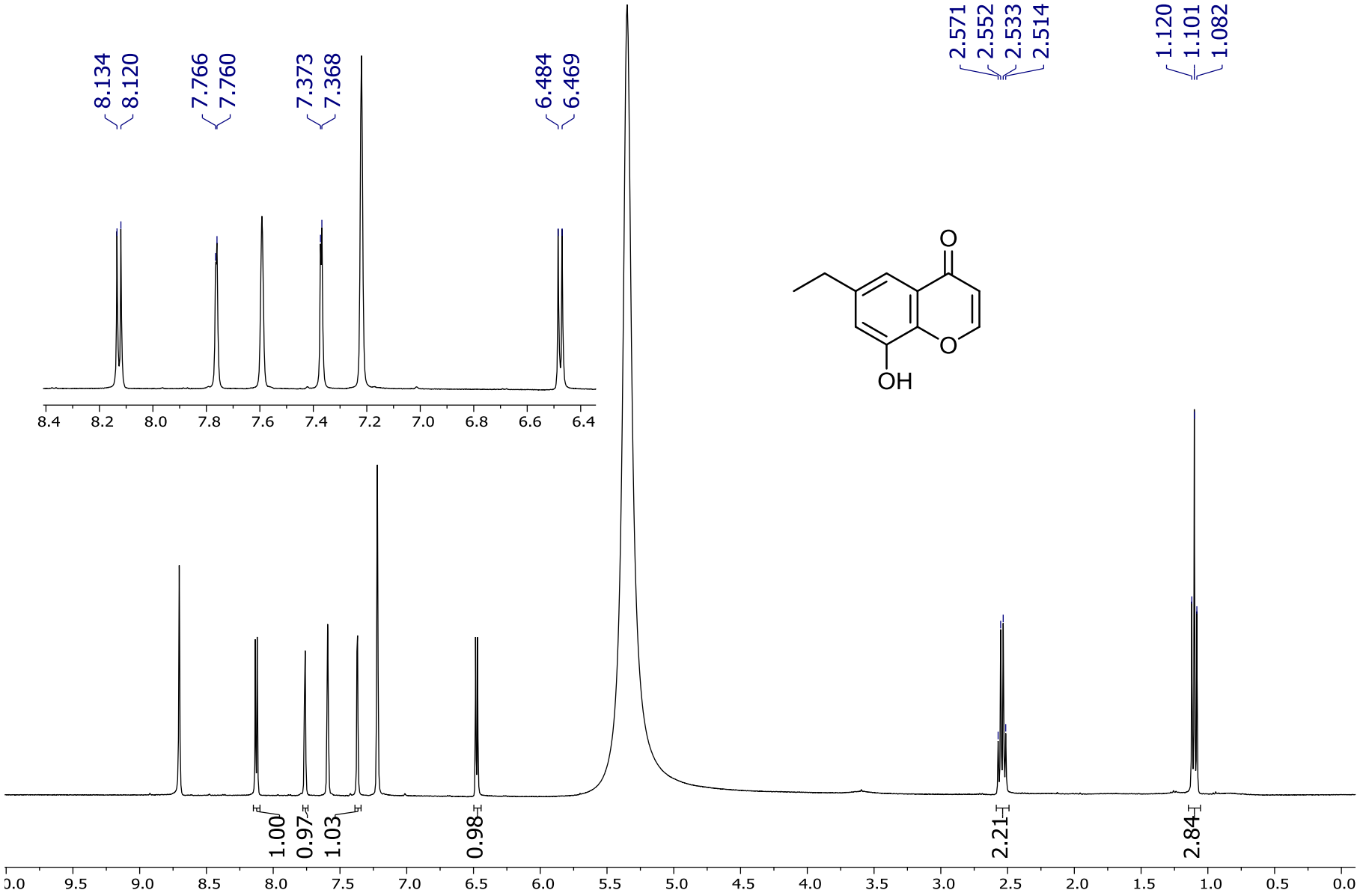

Figure S2. ^{1}H NMR spectrum of **1**.

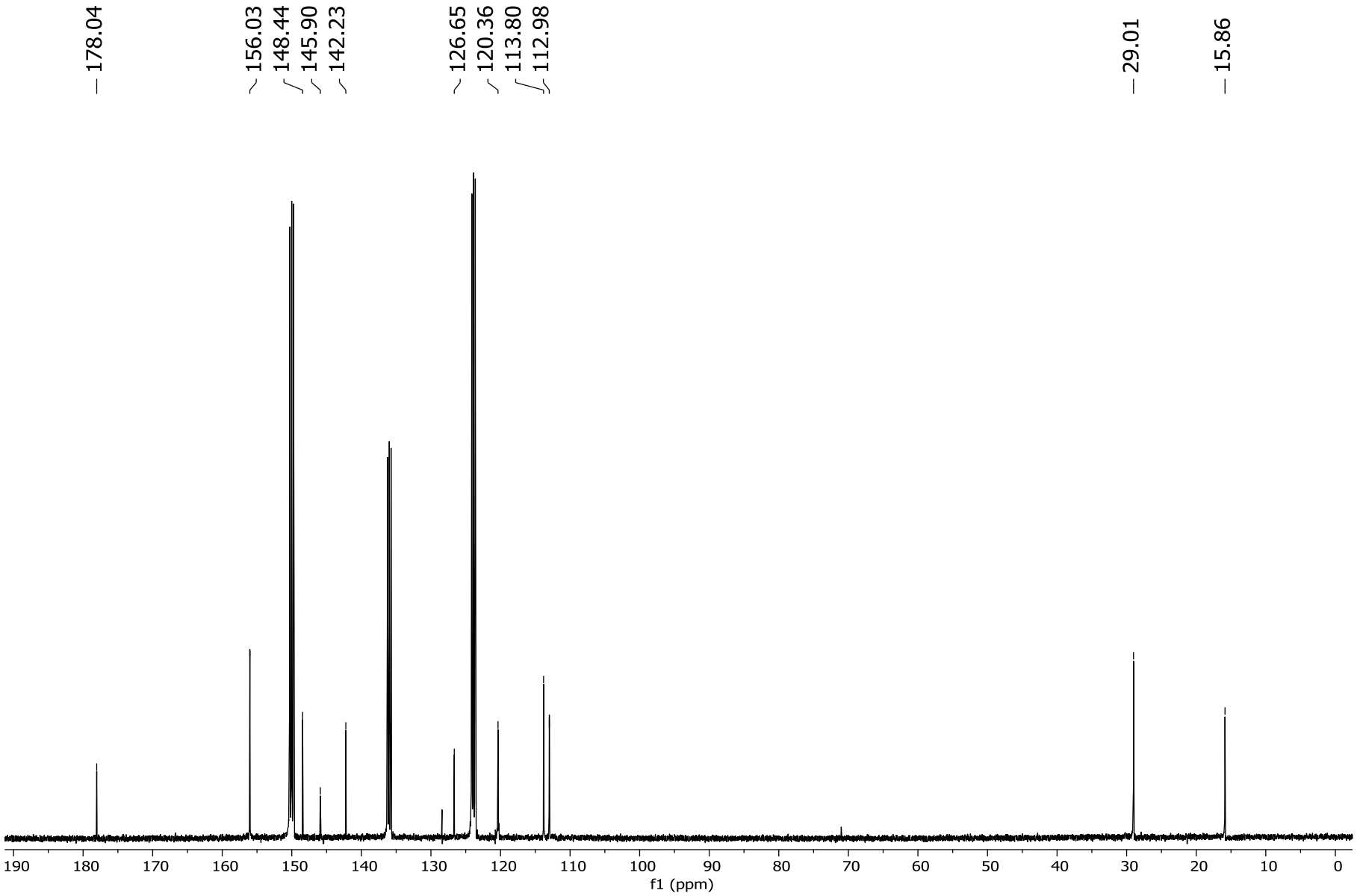

Figure S3. ^{13}C NMR spectrum of **1**.

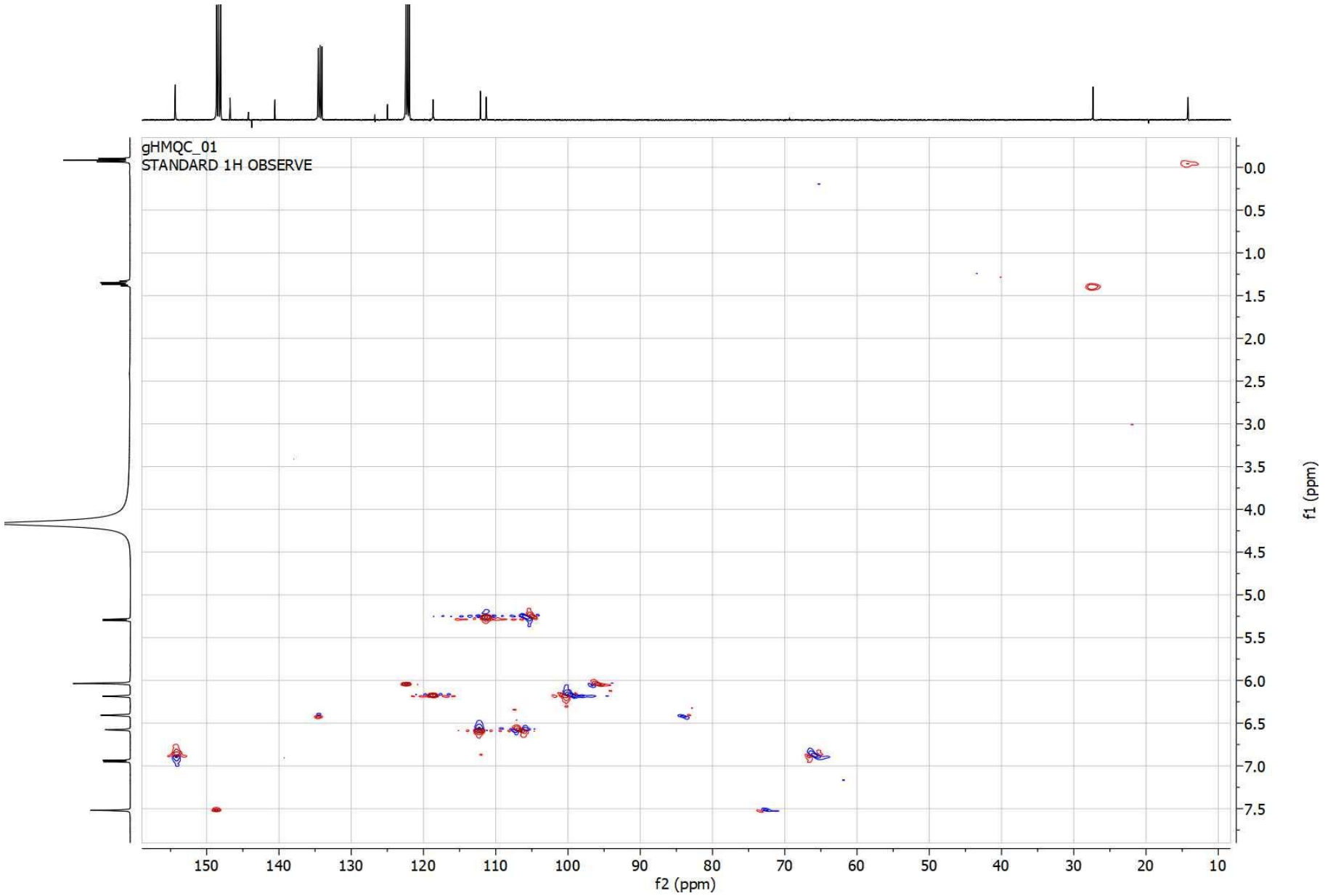

Figure S4. HMQC spectrum of **1**.

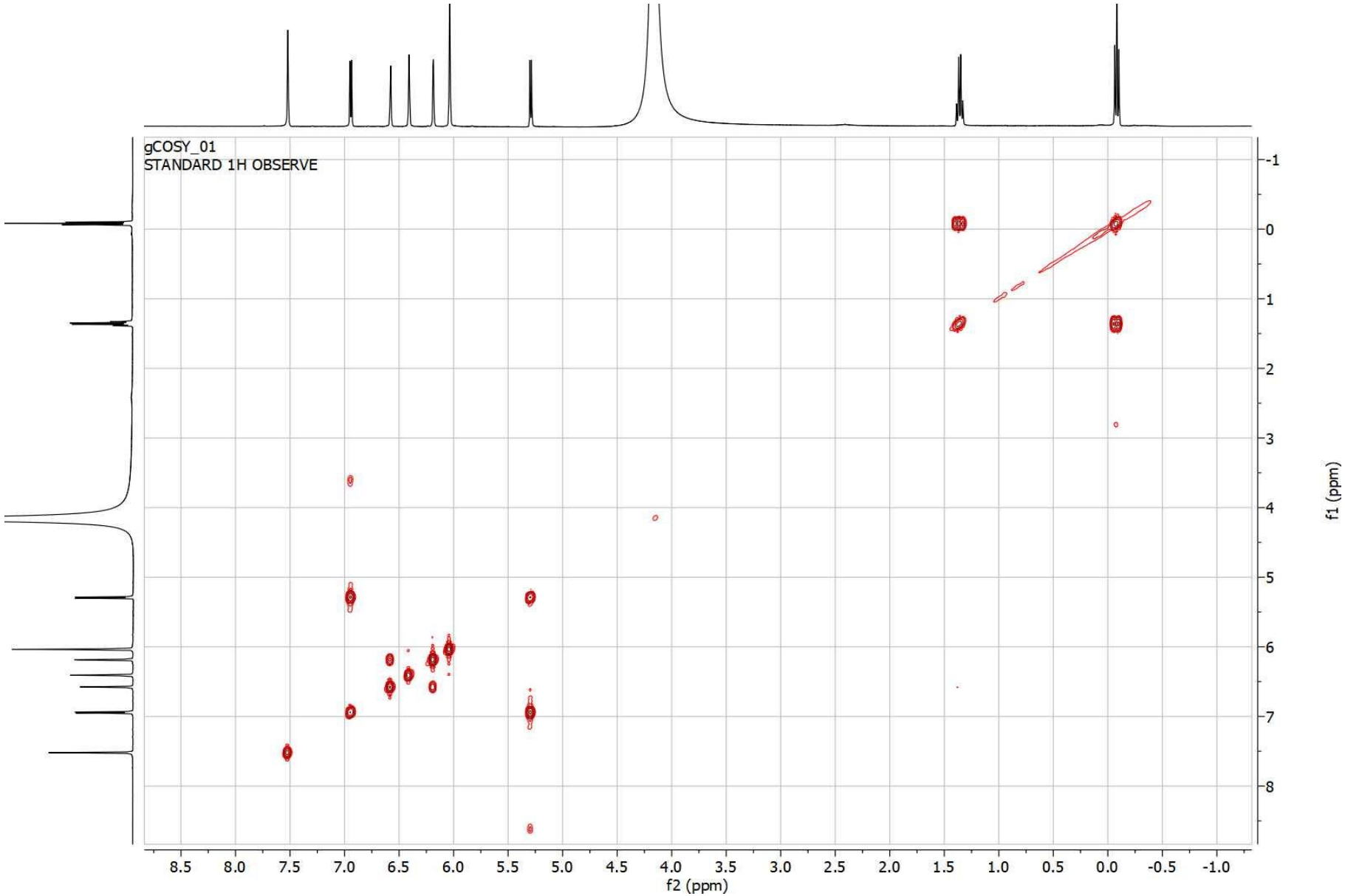

Figure S5. COSY spectrum of **1**.

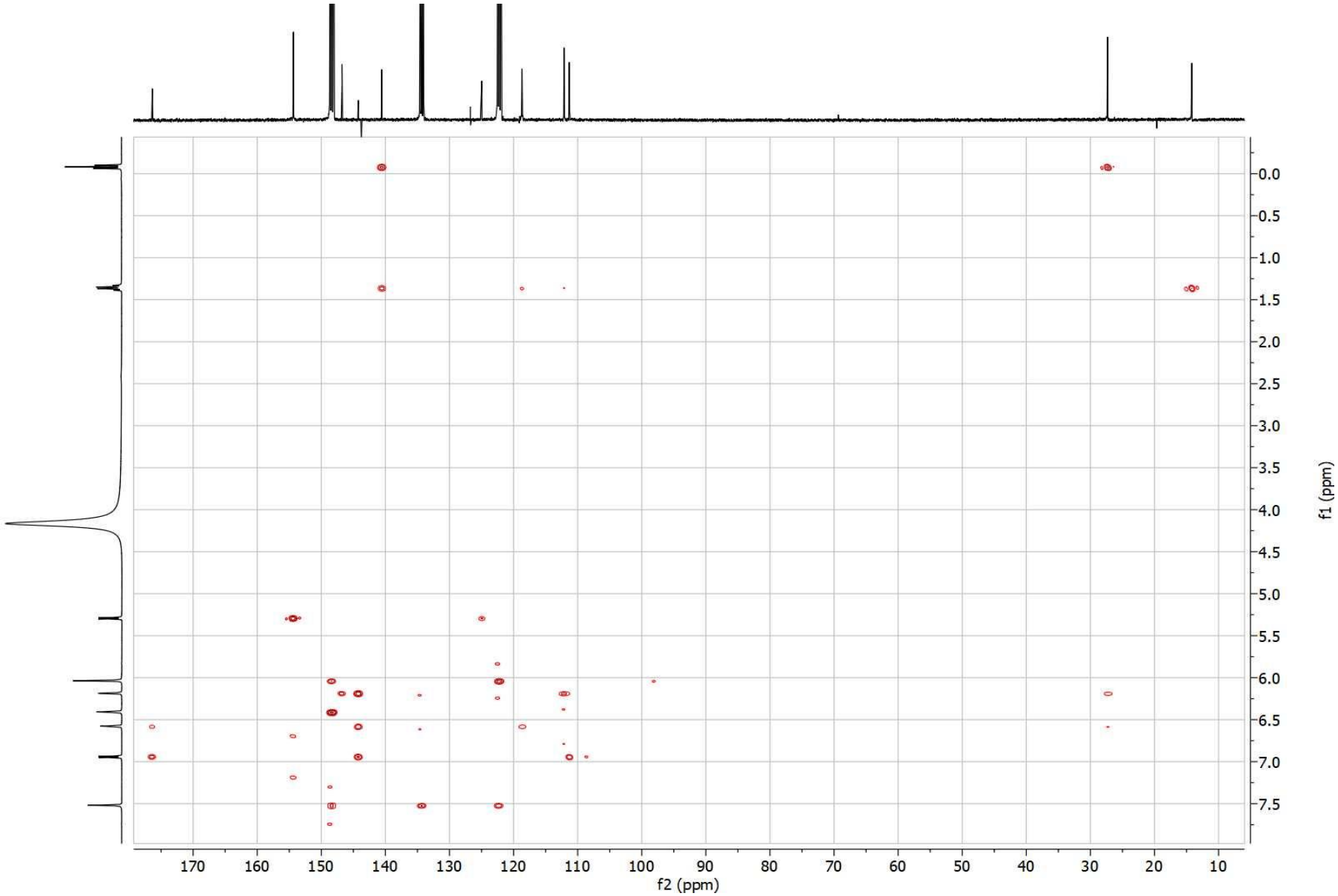

Figure S6. HMBC spectrum of **1**.

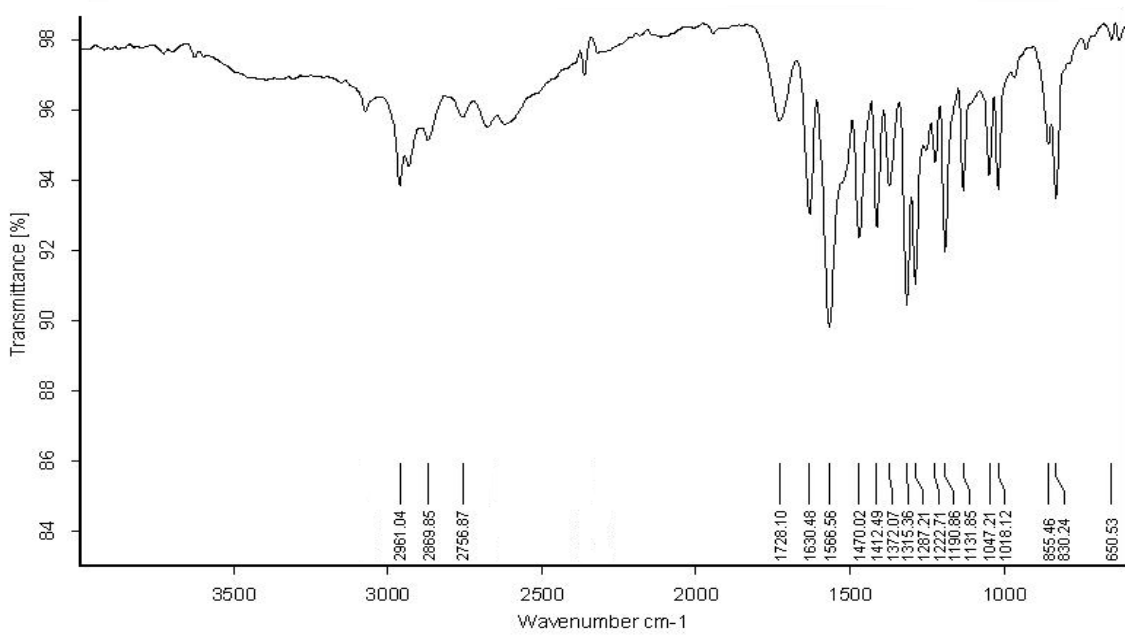

Figure S7. IR spectrum of **1**.

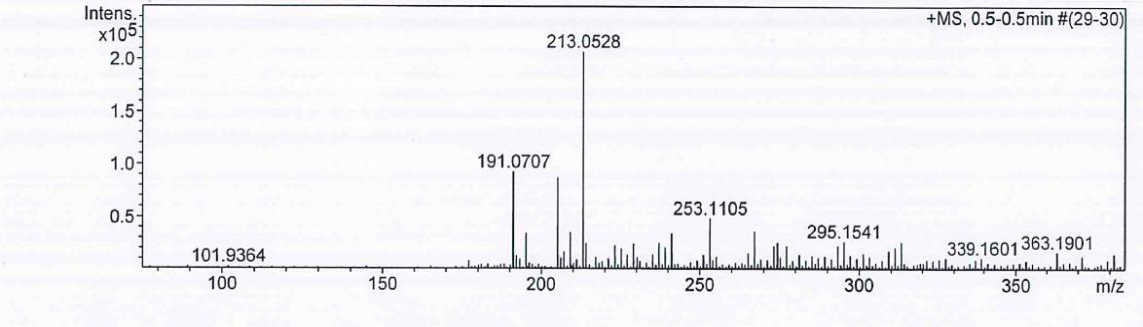

Figure S8. HR-ESI-MS spectrum of **1**.

Table S2. The ^{1}H and ^{13}C NMR data of **2** (400 MHz, Methanol-d_4) and COSY and HMBC spectral data of **2**

Position		δ_H	δ_C	**COSY**	**HMBC**
1					
2	CH	8.09 (d, 5.9)	155.7	3	3, 4, 8a
3	CH	6.24 (d, 5.9)	110.9	2	2, 4, 4a
4	C		178.6		
4a	C		116.5		
5	CH	7.42 (s)	114.2		4, 7, 9, 8a
6	C		130.3		
7	C		149.3		
8	C		131.9		
8a	C		145.9		
9	CH_2	2.71 (q, 7.5)	22.7	12	5, 6, 7, 10
10	CH_3	1.23 (t, 7.5)	12.8	11	6, 9

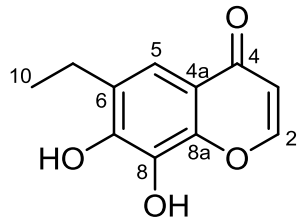

Figure S9. Structure of compound **2**.

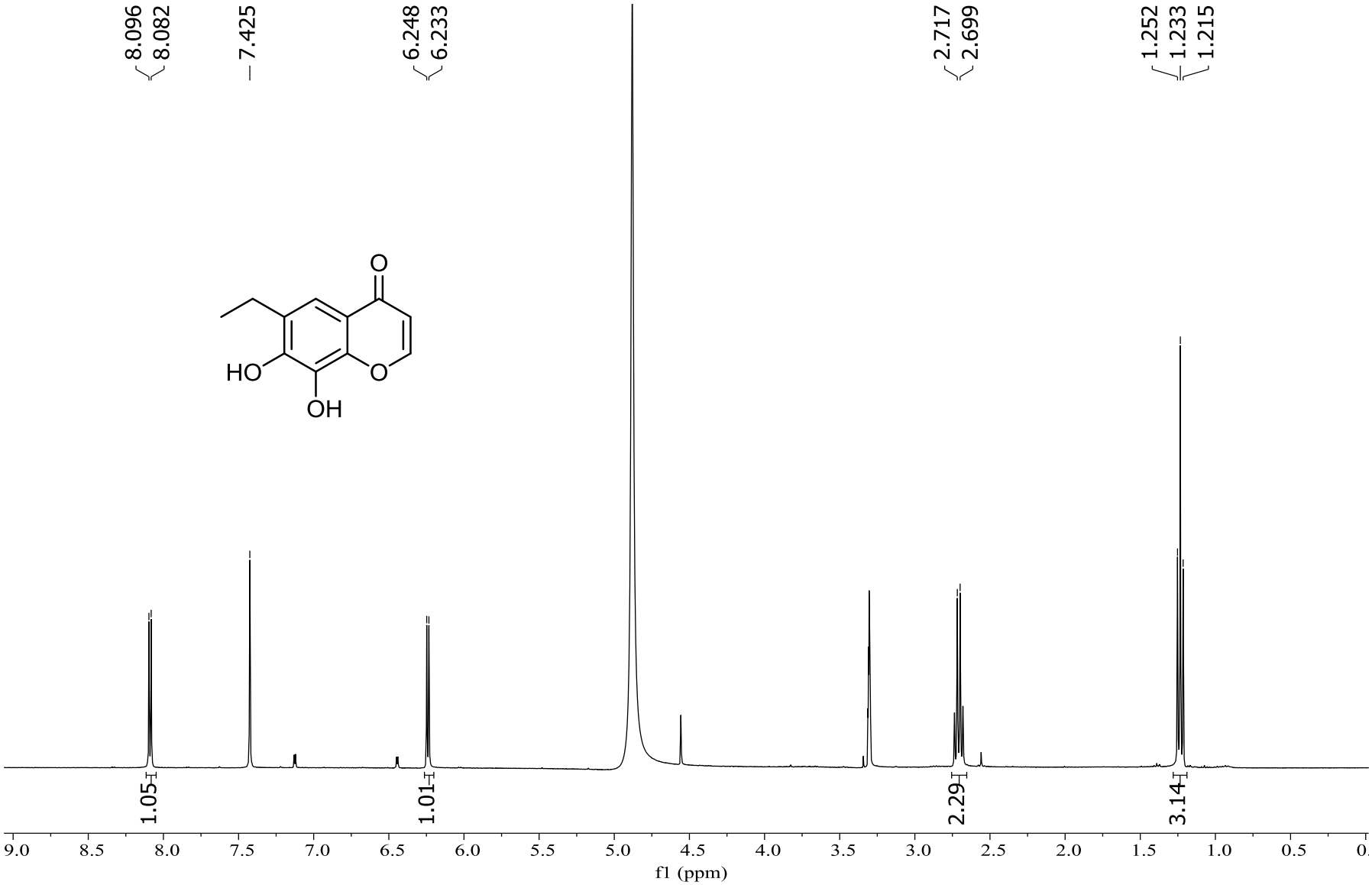

Figure S10. ^{1}H NMR spectrum of **2**.

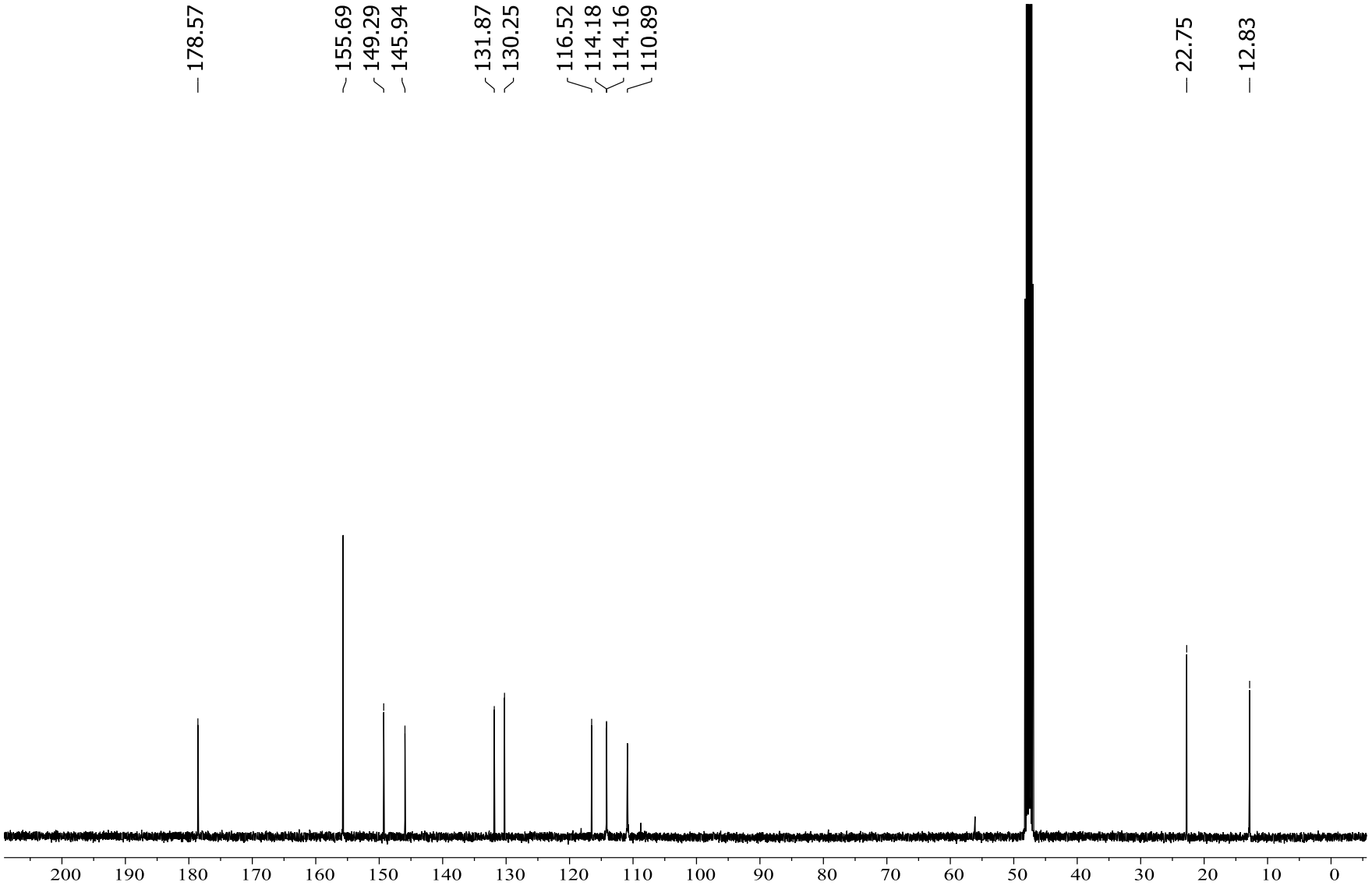

Figure S11. ^{13}C NMR spectrum of **2**.

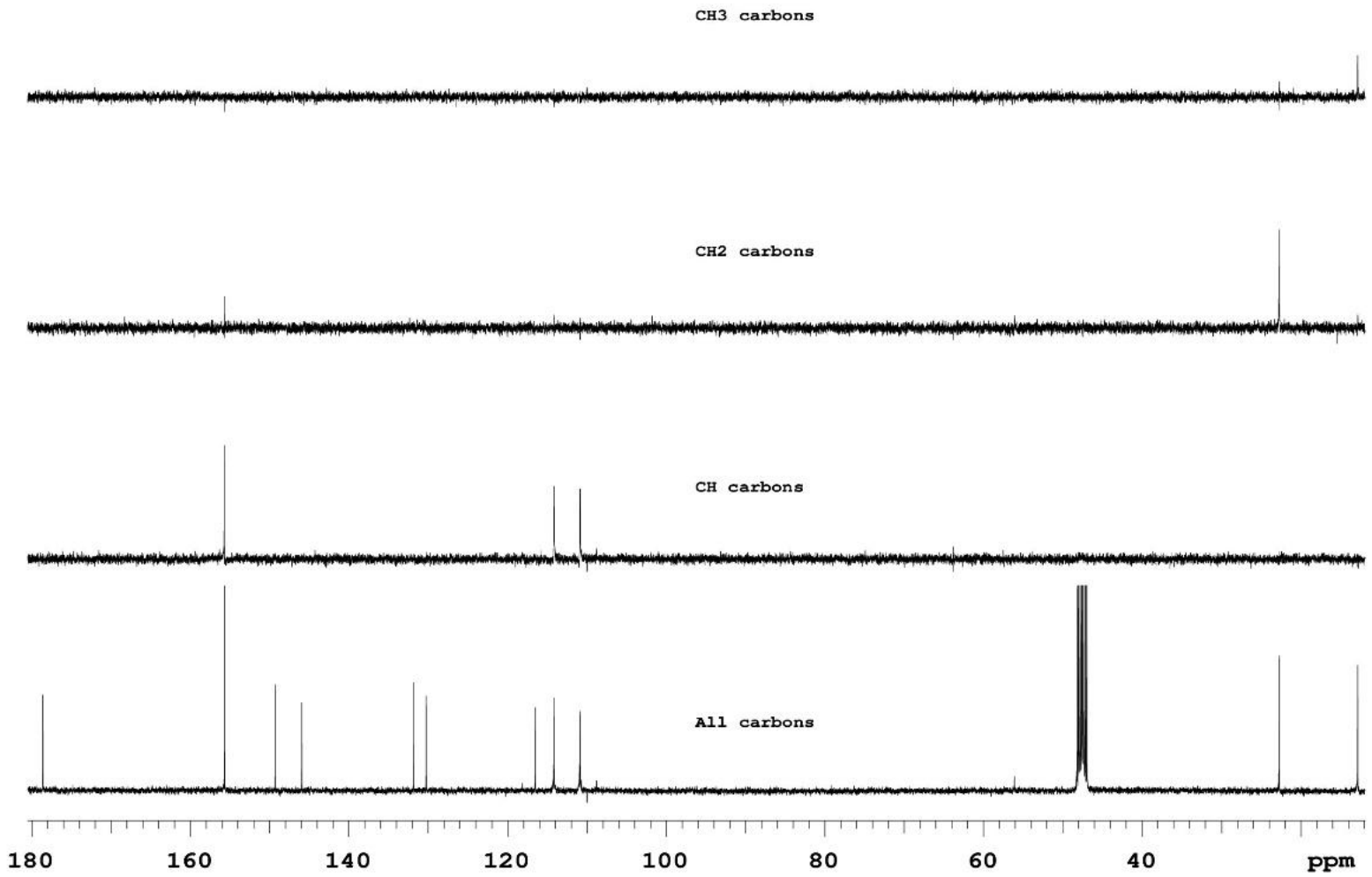

Figure S12. DEPT spectrum of **2**.

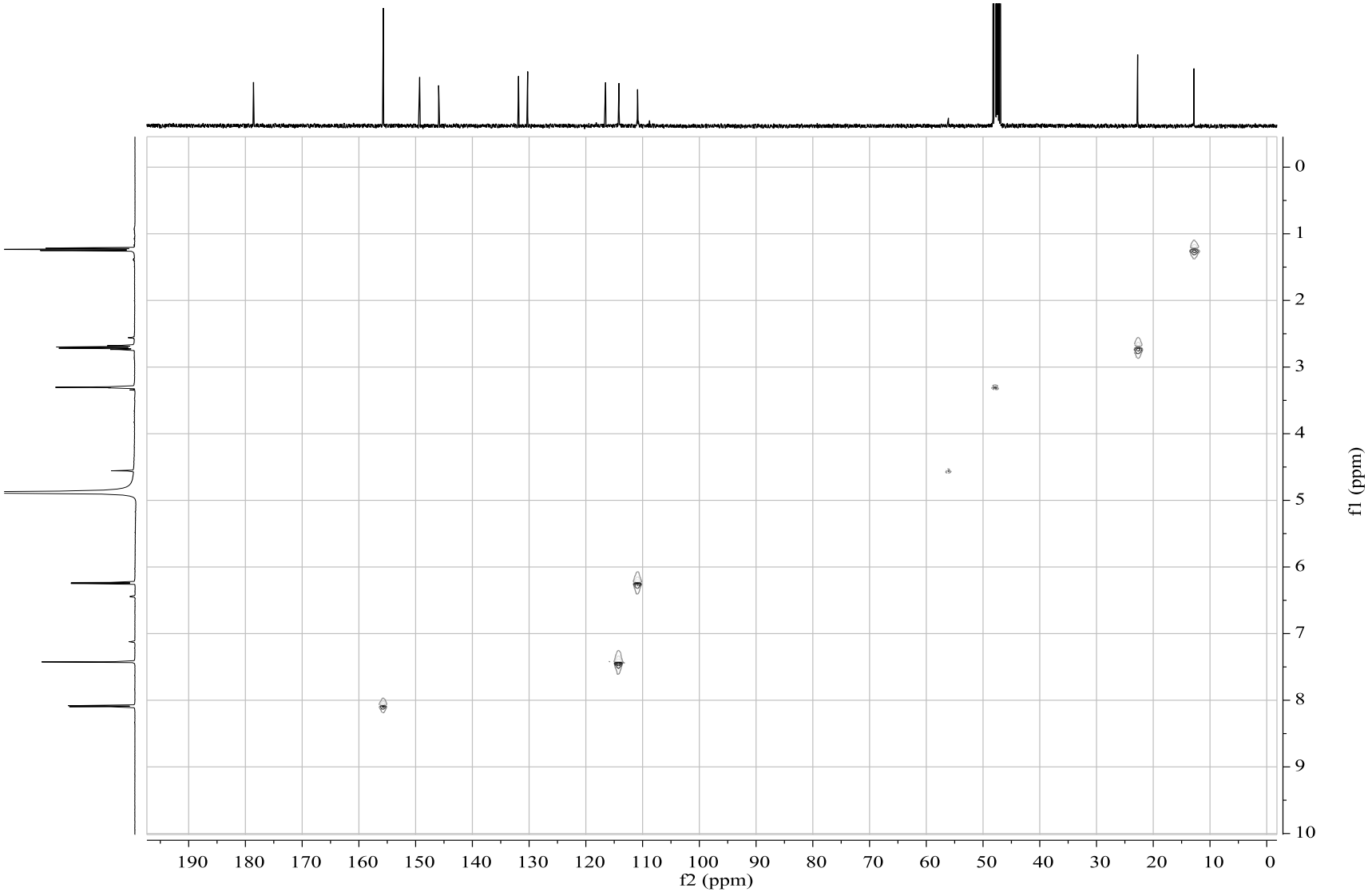

Figure S13. HMQC spectrum of **2**.

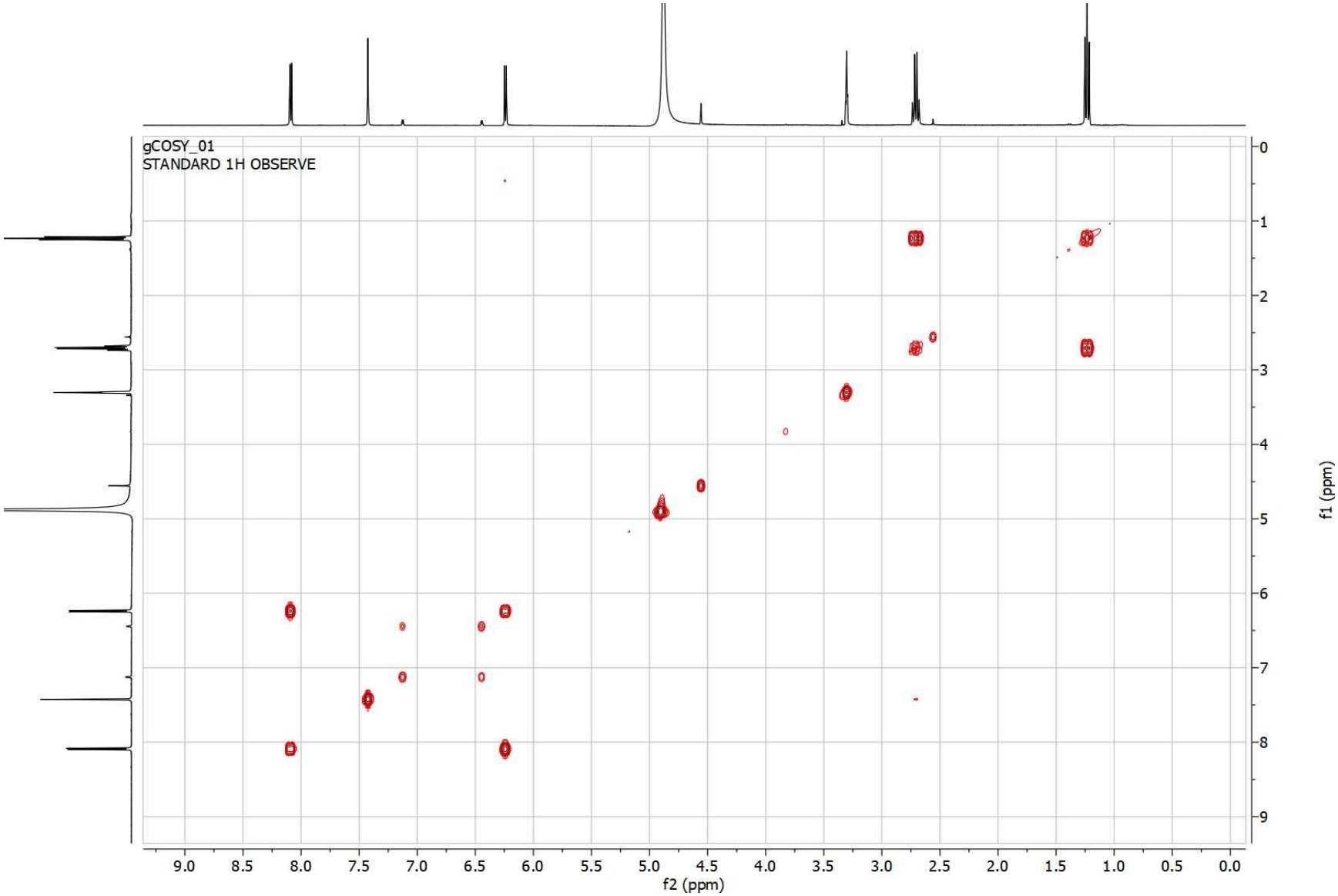

Figure S14. COSY spectrum of **2**.

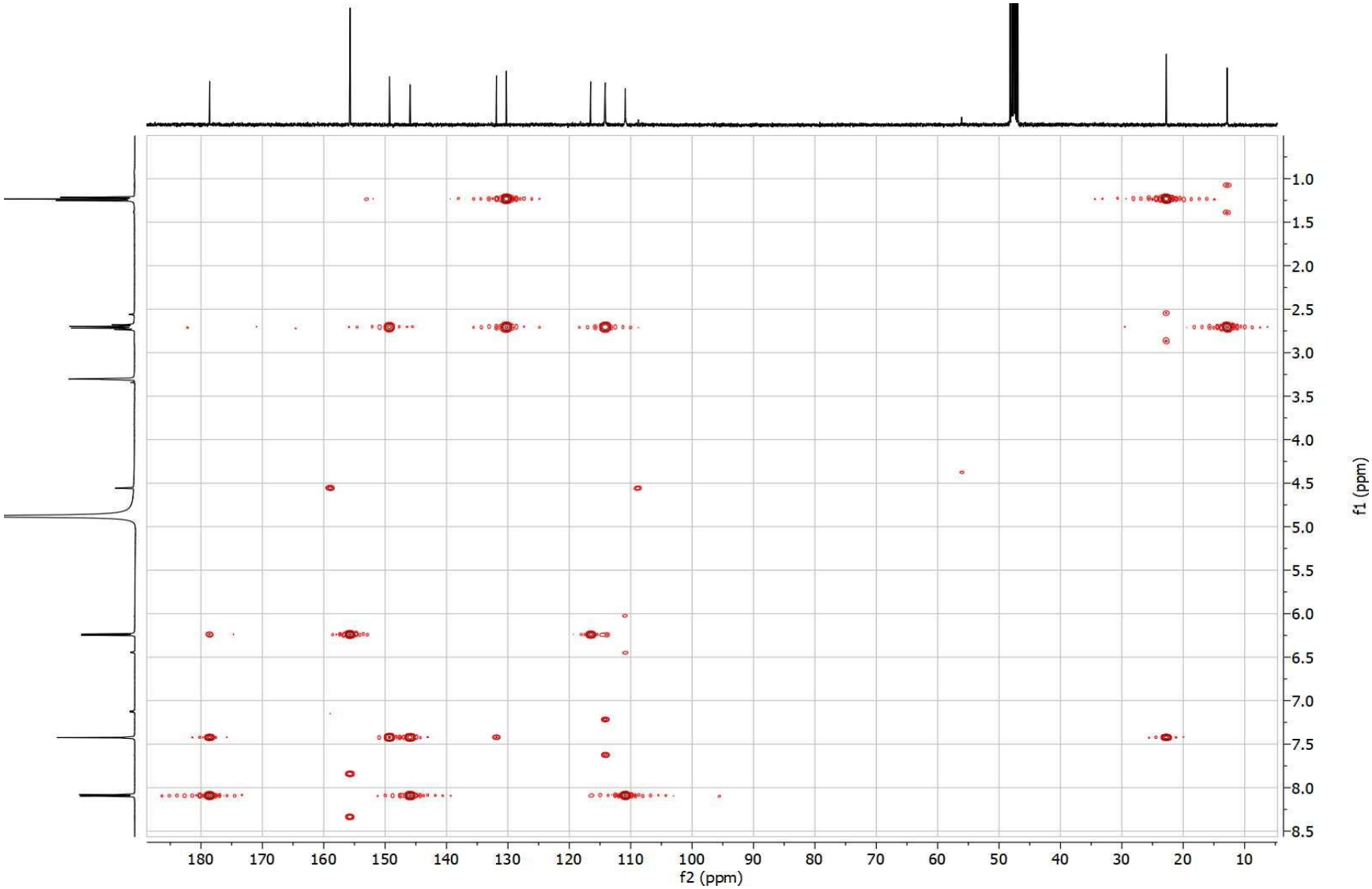

Figure S15. HMBC spectrum of **2**.

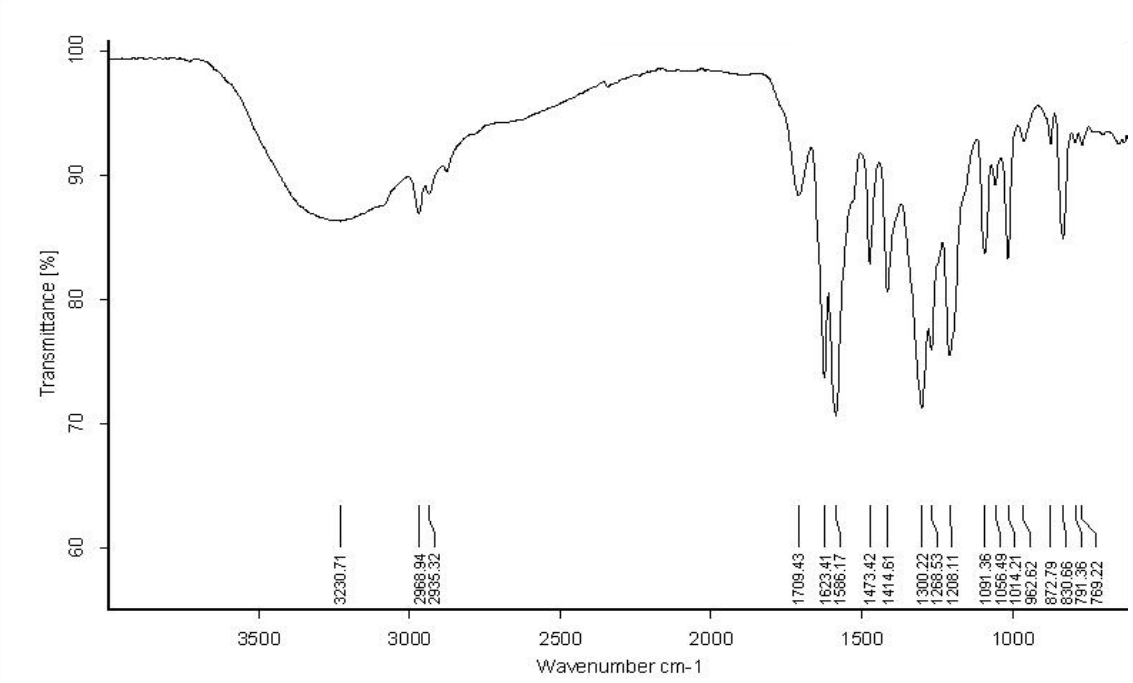

Figure S16. IR spectrum of **2**.

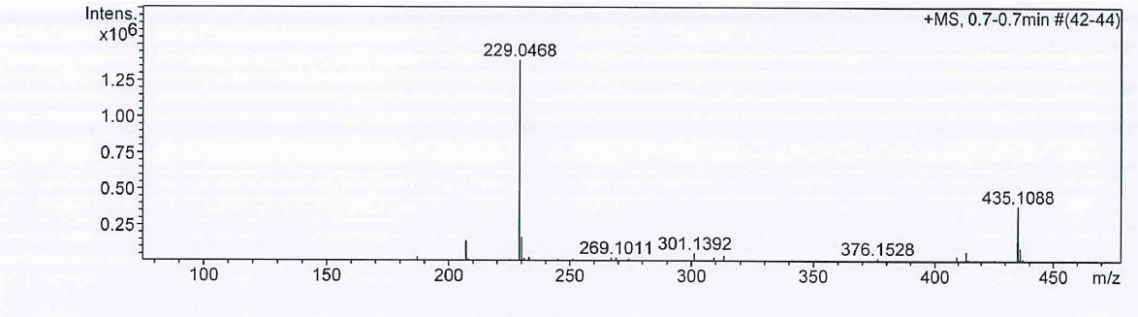

Figure S17. HR-ESI-MS of **2**.

Table S3. The ^{1}H and ^{13}C NMR data of **3** (400 MHz, $CDCl_3$) and COSY, and HMBC spectral data of **3**

Position	δ_H	δ_C	**COSY**	**HMBC**
1 C		170.2		
2 O				
3 CH	4.71 (dsext, 6.4, 2.1)	76.7	4, 3-CH_3	
4 CH_2	2.87 (m)	34.1	3	3, 4a, 5, 8a, 3-CH_3
4a C		130.0		
5 CH	6.63 (d, 8.0)	116.8	6	4, 7, 8a
6 CH	7.00 (d, 8.1)	117.5	5	4a, 7, 8
7 C		147.4		
8 C		152.5		
8a C		108.3		
3-CH_3	1.51 (d, 6.3)	20.7	3	3, 4
7-OCH_3	3.88 (s)	56.3		7
8-OH	11.23 (s)			7, 8, 8a

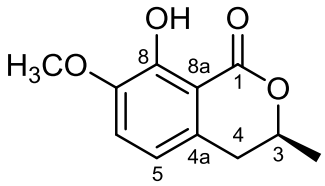

Figure S18. Structure of compound **3**.

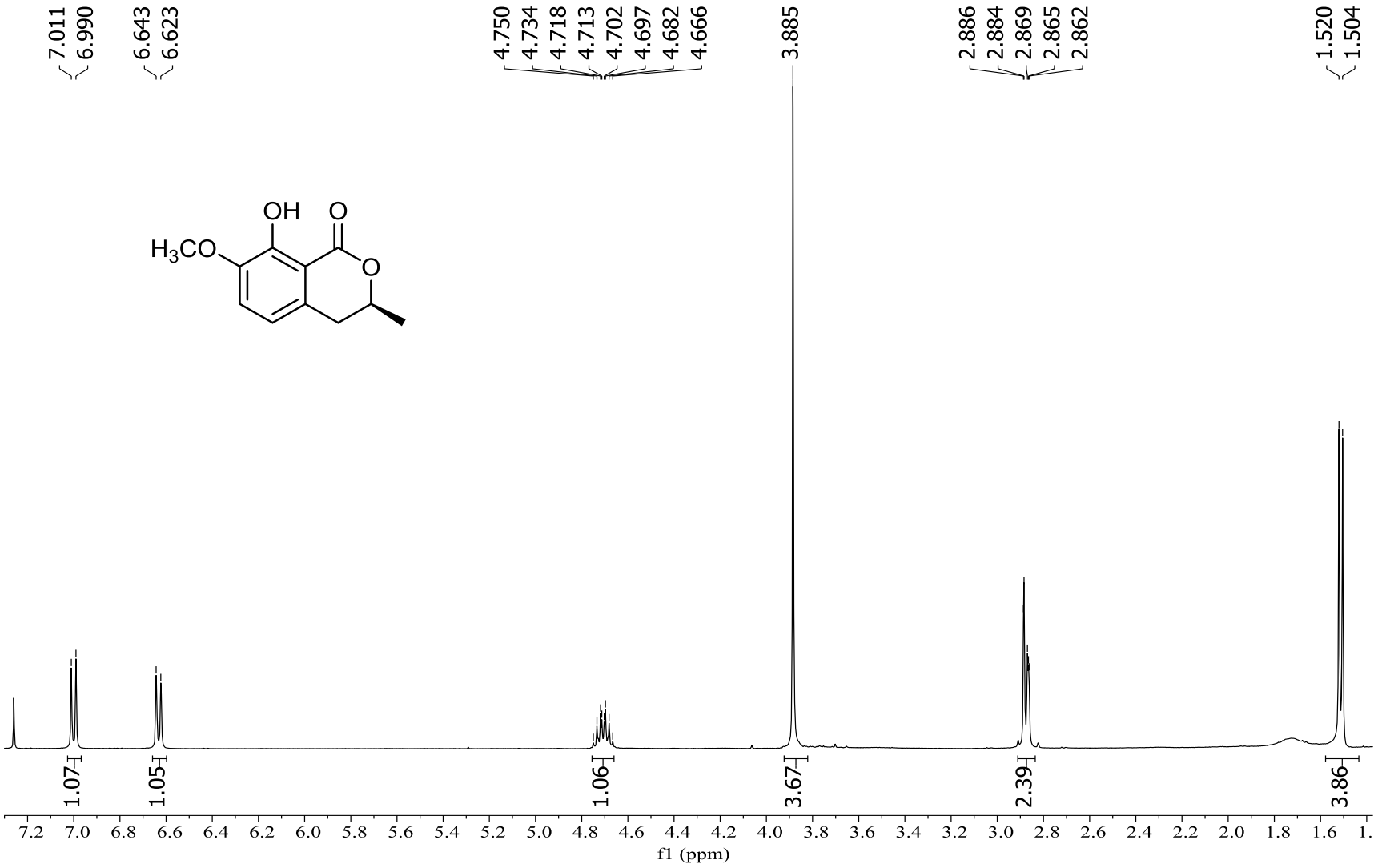

Figure S19. ^{1}H NMR spectrum of **3**.

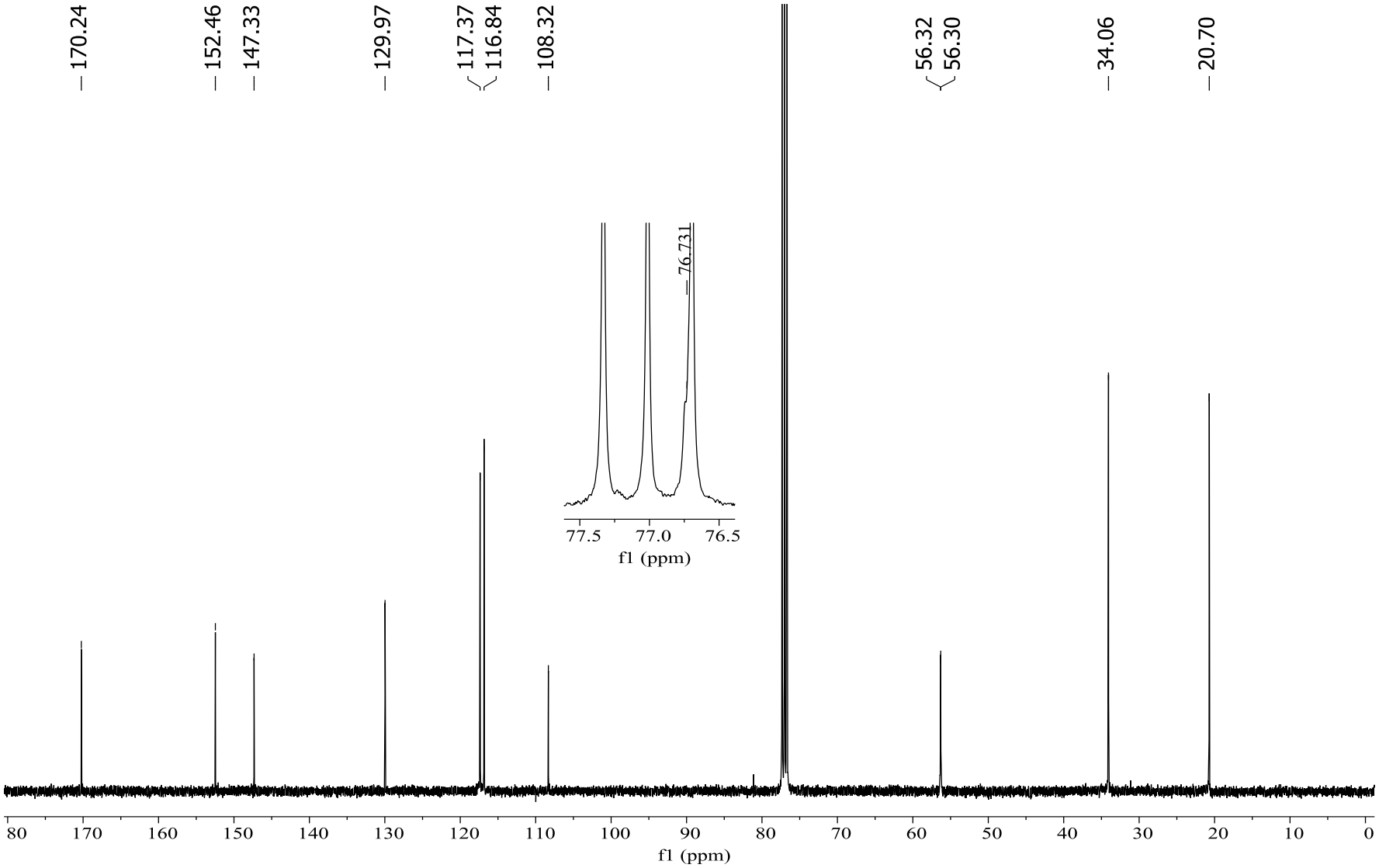

Figure S20. ^{13}C NMR spectrum of **3**.

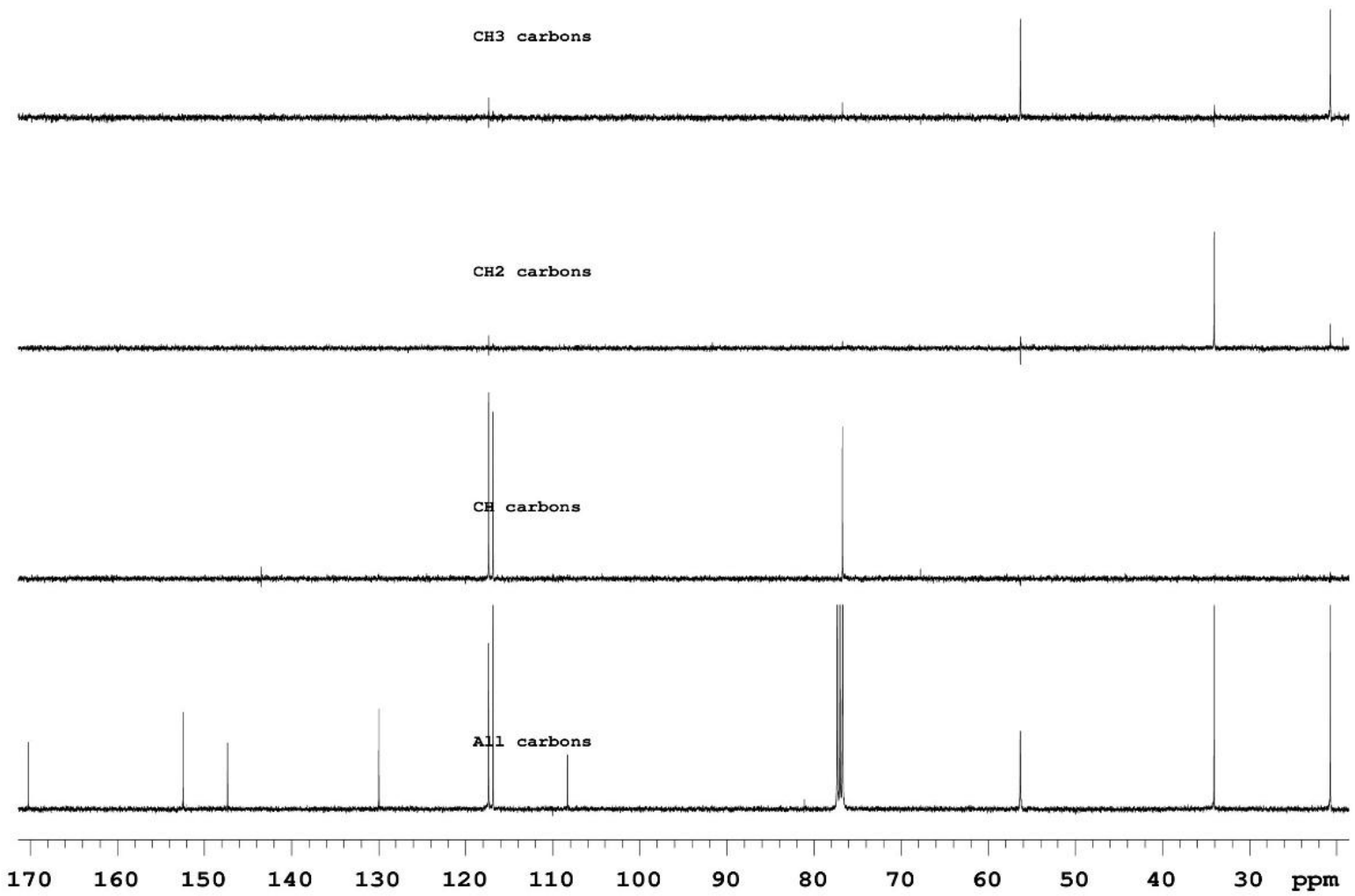

Figure S21. DEPT spectrum of **3**.

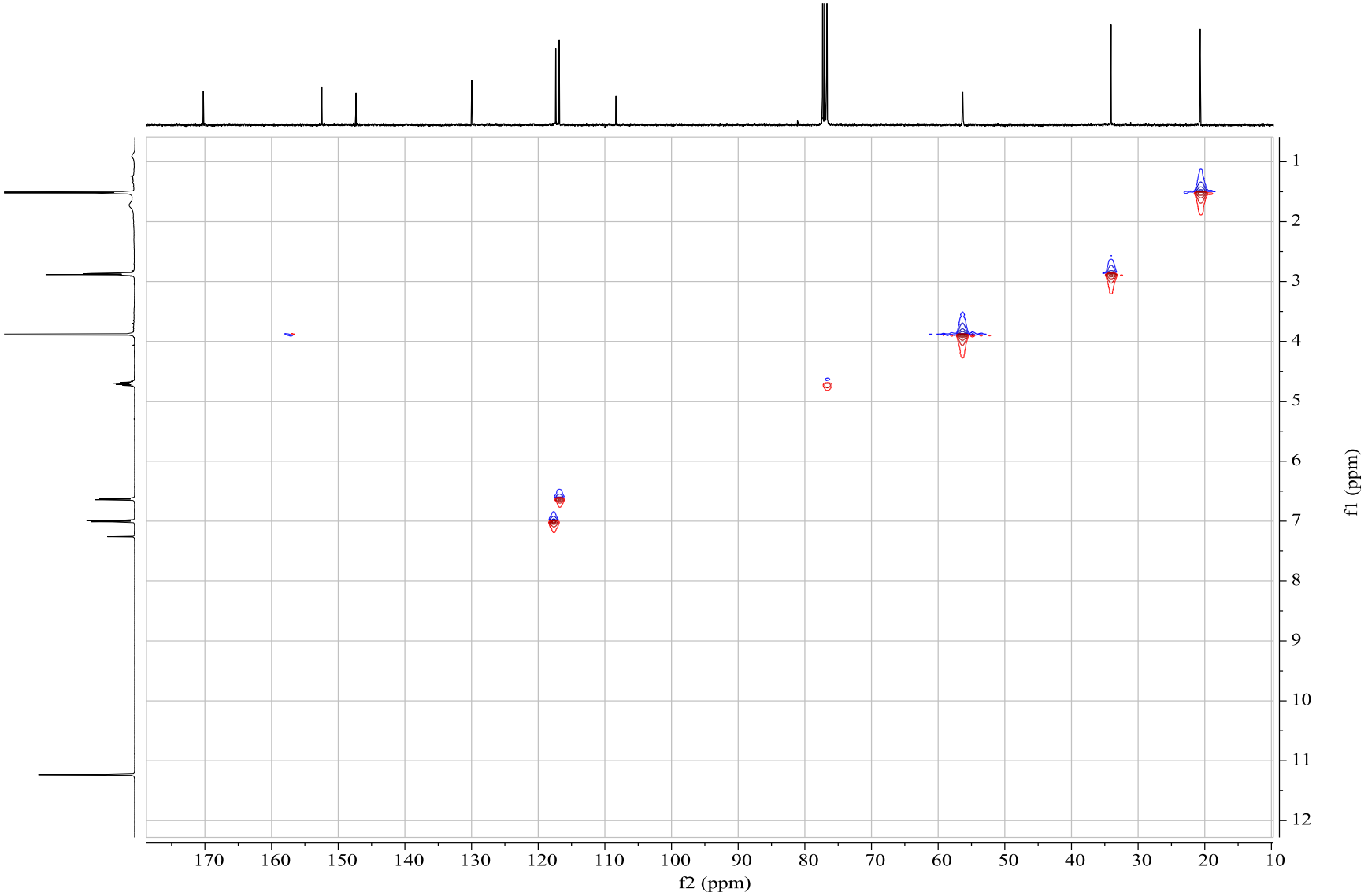

Figure S22. HMQC spectrum of **3**.

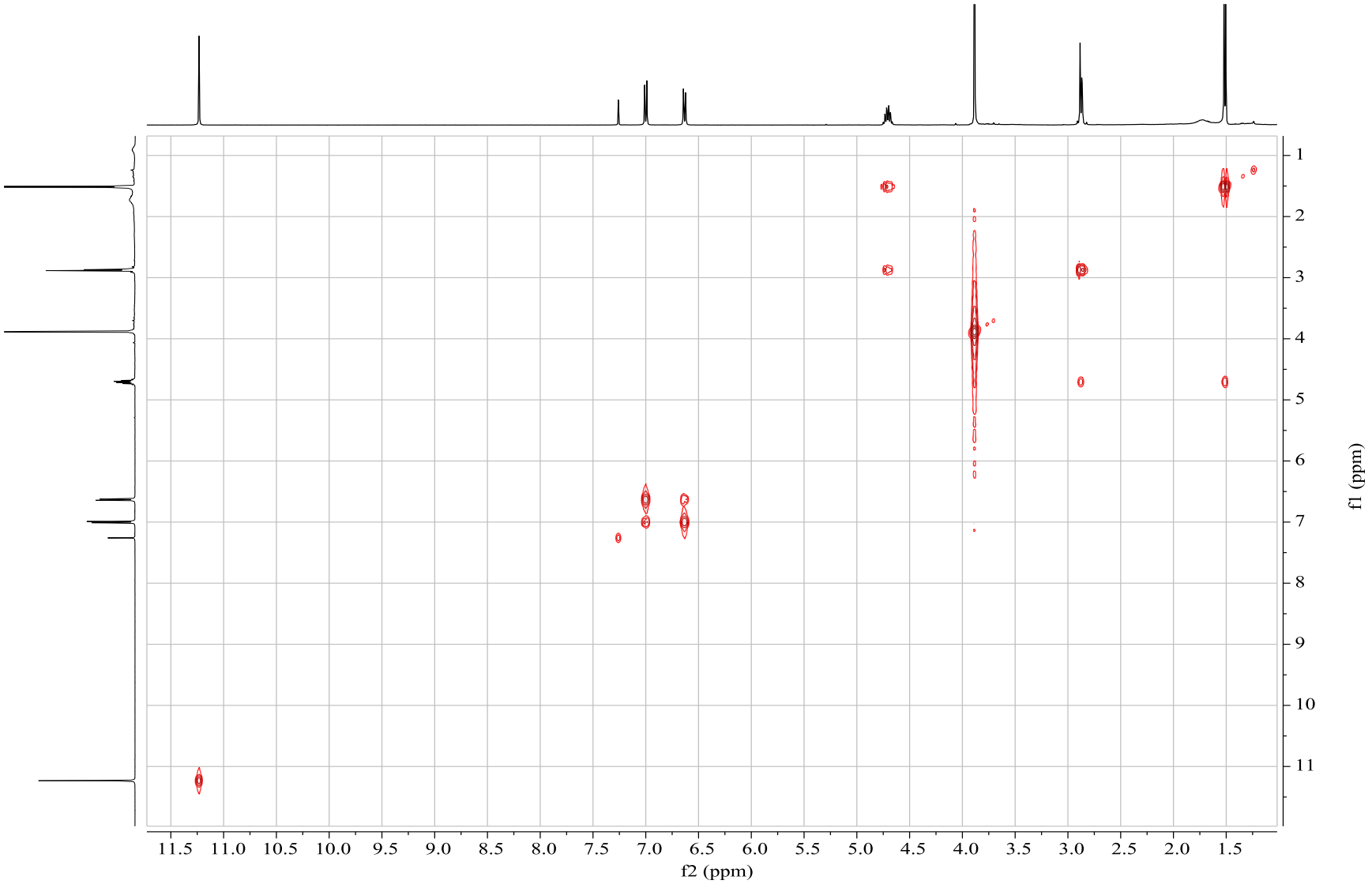

Figure S23. COSY spectrum of **3**.

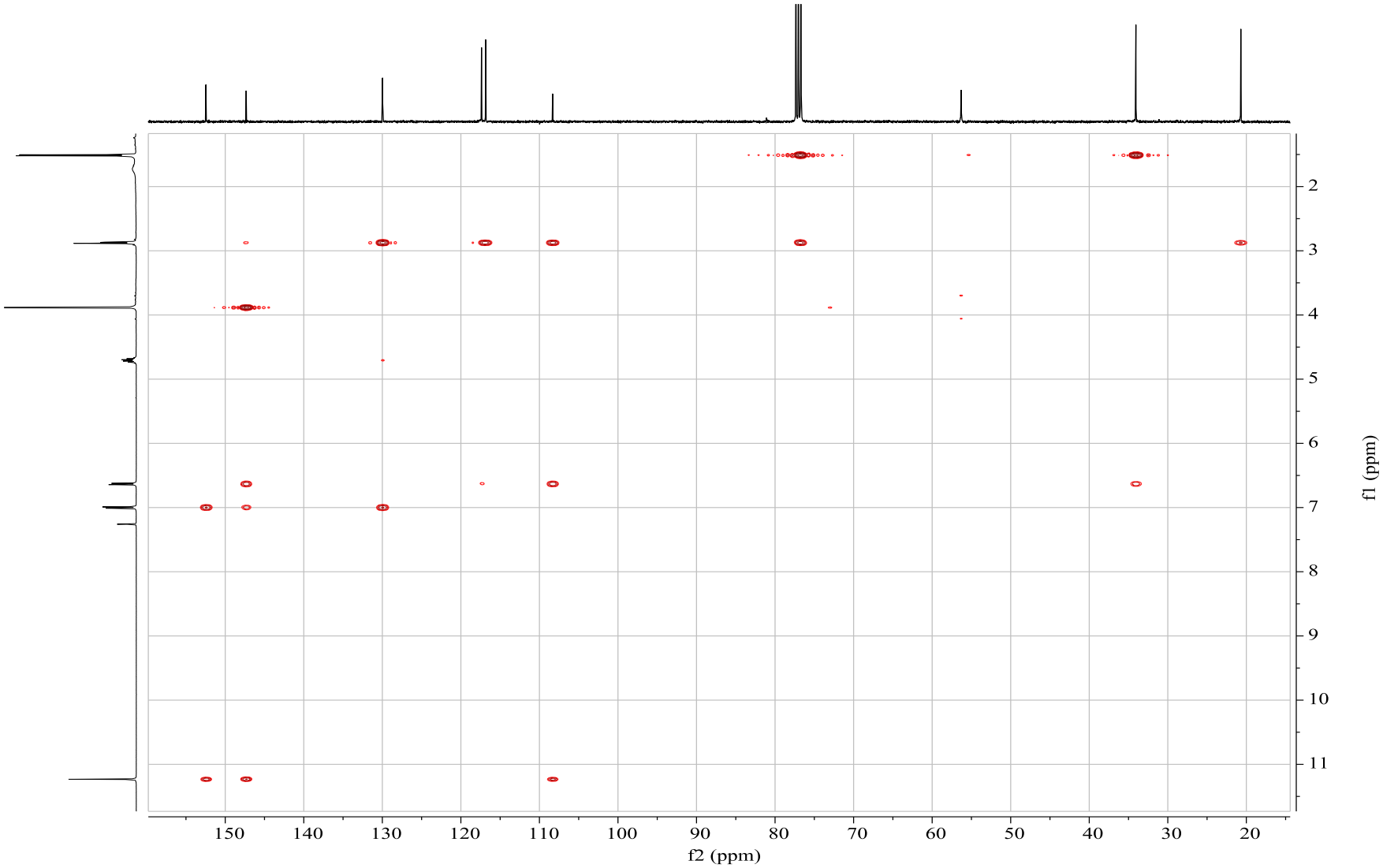

Figure S24. HMBC spectrum of **3**.

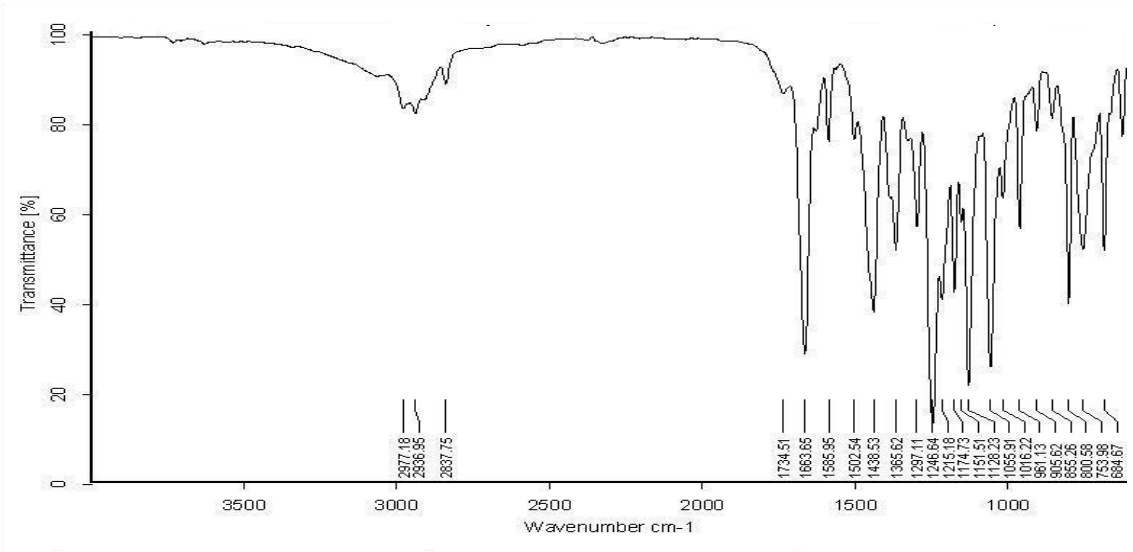

Figure S25. IR spectrum of **3**.

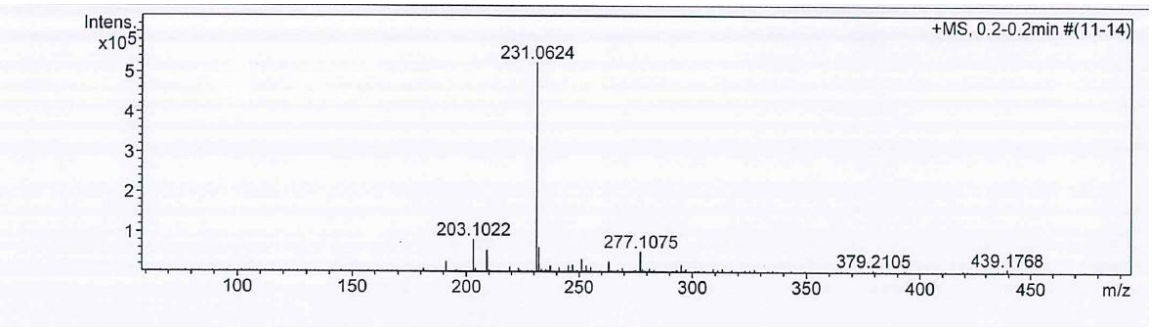

Figure S26. HR-ESI-MS of **3**.

(3*R*)-**3**

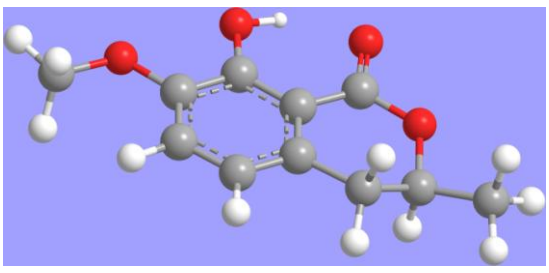

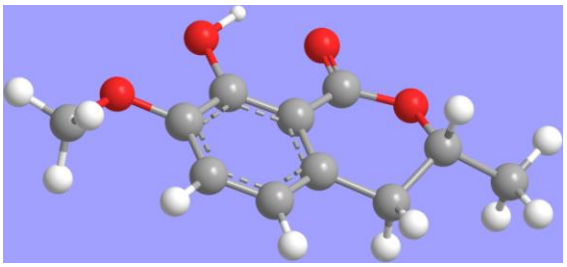

Figure S27. The global minimum energy conformers and the percentage of Boltzmann popularity of (3*R*)-**3** and (3*S*)-**3.**

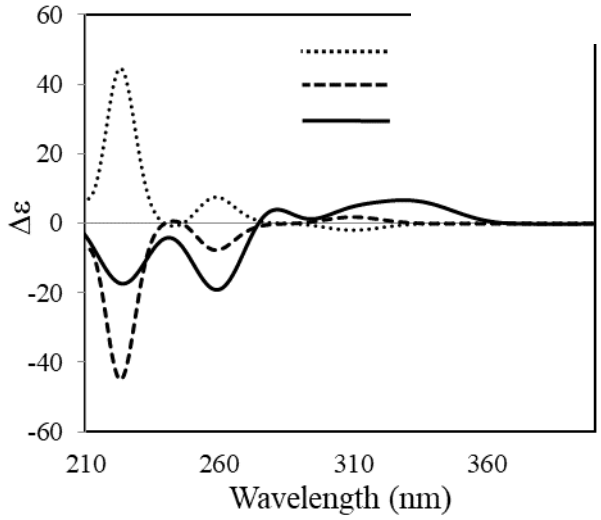

Figure S28. Comparison of calculated ECD and experimental spectra of **3**.

Table S4. The ^{1}H and ^{13}C NMR data of **4** (400 MHz, Methanol-d_4) and COSY and HMBC spectral data of **4**.

Position		**δ_H**	**δ_C**	**COSY**	**HMBC**
1	C		170.7		
2	O				
3	CH	4.66 (dqd, 12.5, 6.4, 3.6)	76.9	4, 3-CH_3	4a
4	CH_2	2.53 (dd, 16.6, 11.4)	27.6	3	3, 4a, 8a, 5,

		3.07 (dd, 16.6, 3.4)			3-CH_3
4a	C		114.0		
5	C		145.2		
6	CH	6.65 (s)	110.3		7, 8, 4a
7	C		144.3		
8	C		143.5		
8a	C		107.6		
3-CH_3		1.48 (d, 6.3)	19.6	3	3, 4

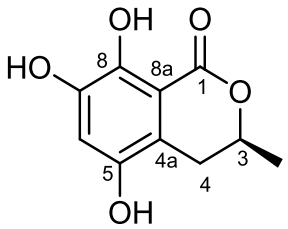

Figure S29. Structure of compound **4**.

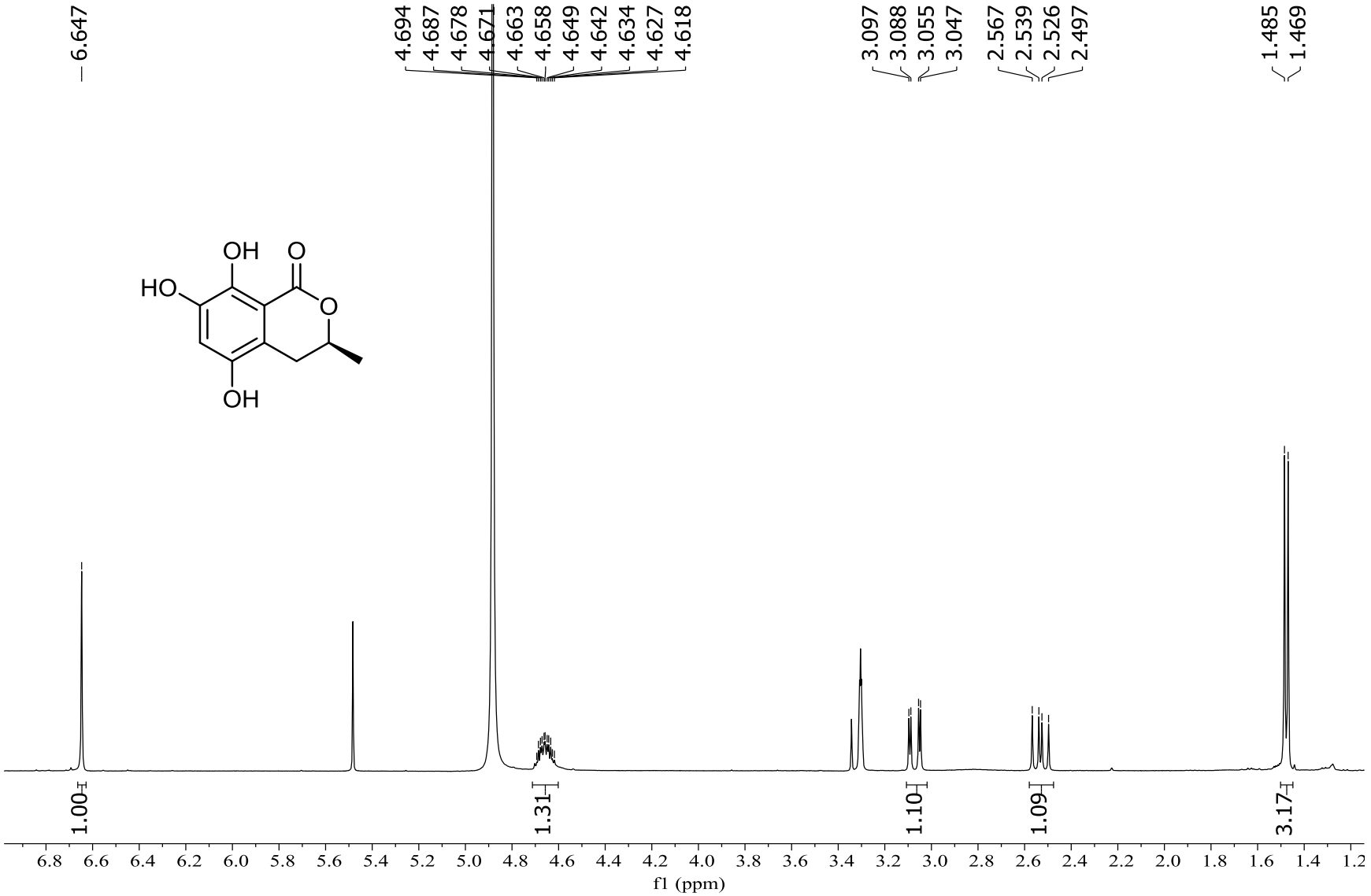

Figure S30. ^{1}H NMR spectrum of **4**.

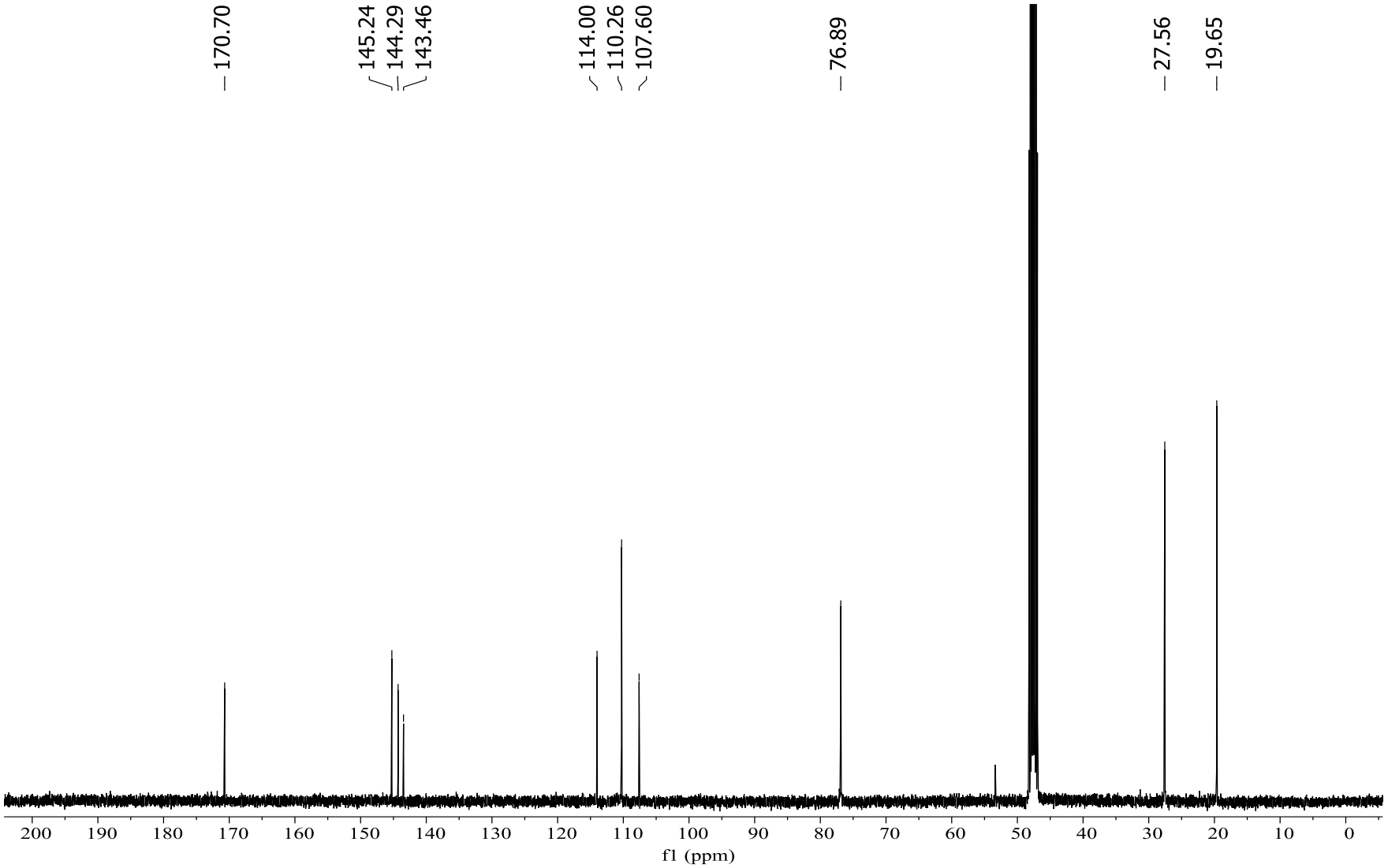

Figure S31. ^{13}C NMR spectrum of **4**.

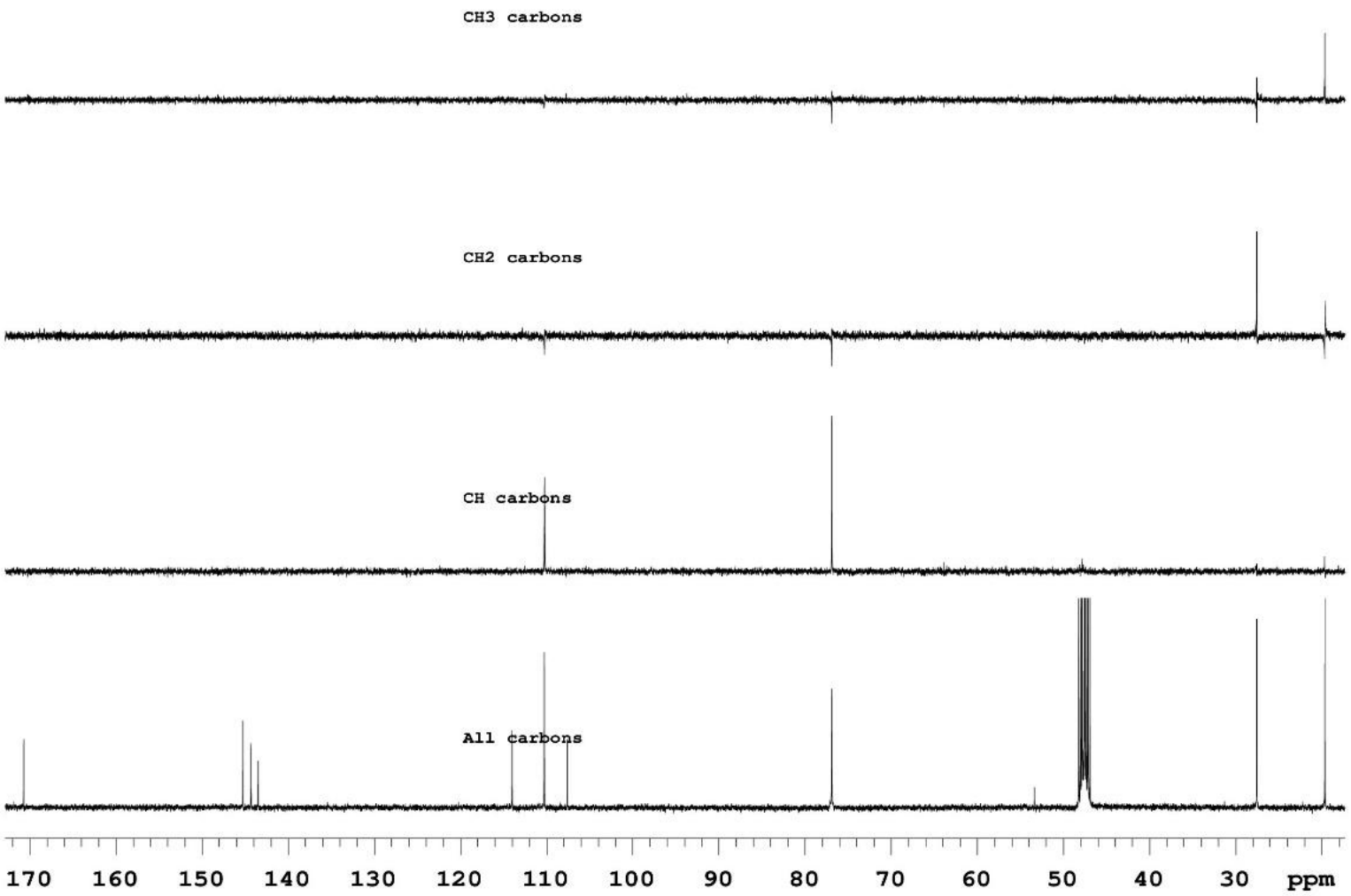

Figure S32. DEPT spectrum of **4**.

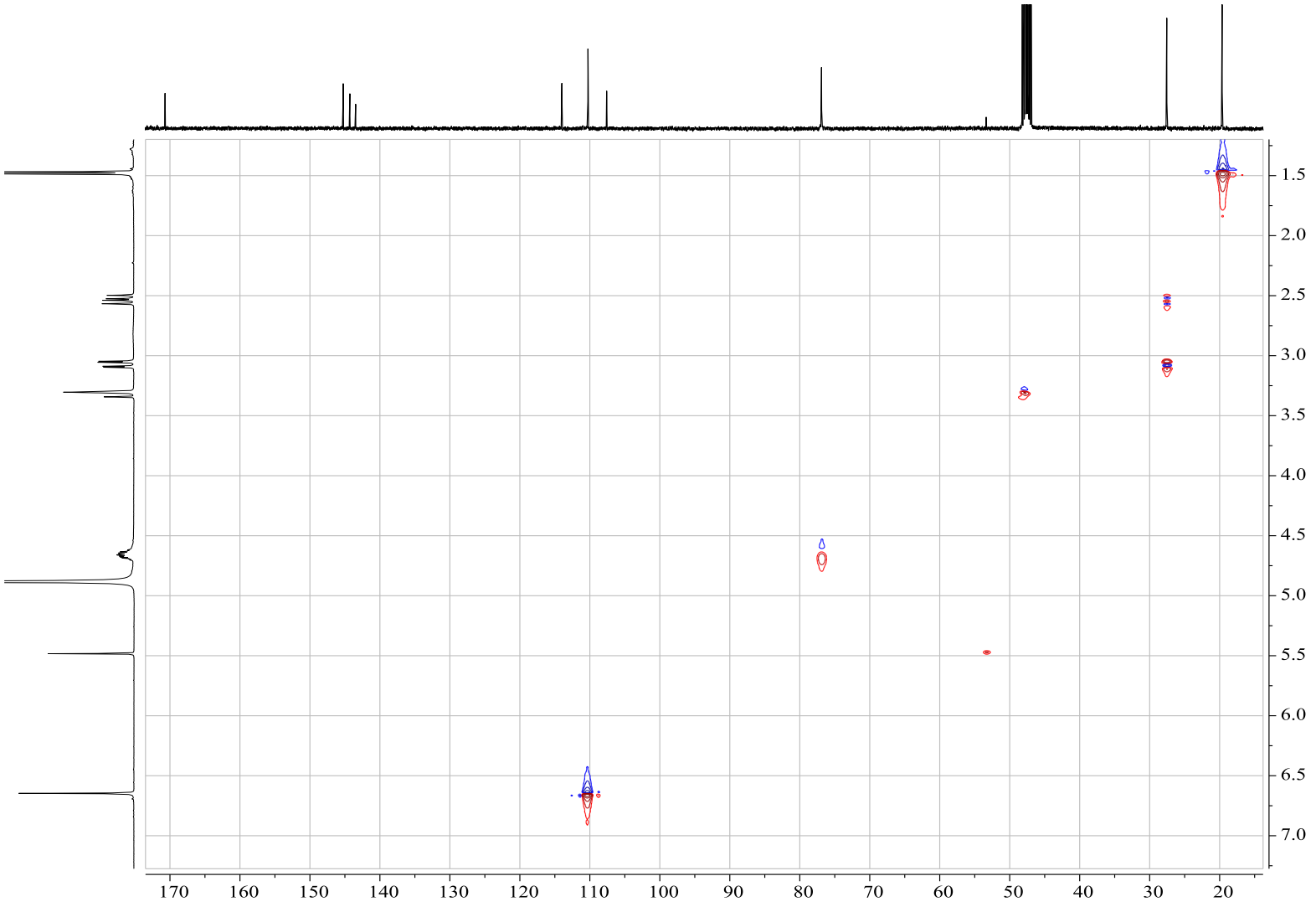

Figure S33. HMQC spectrum of **4**.

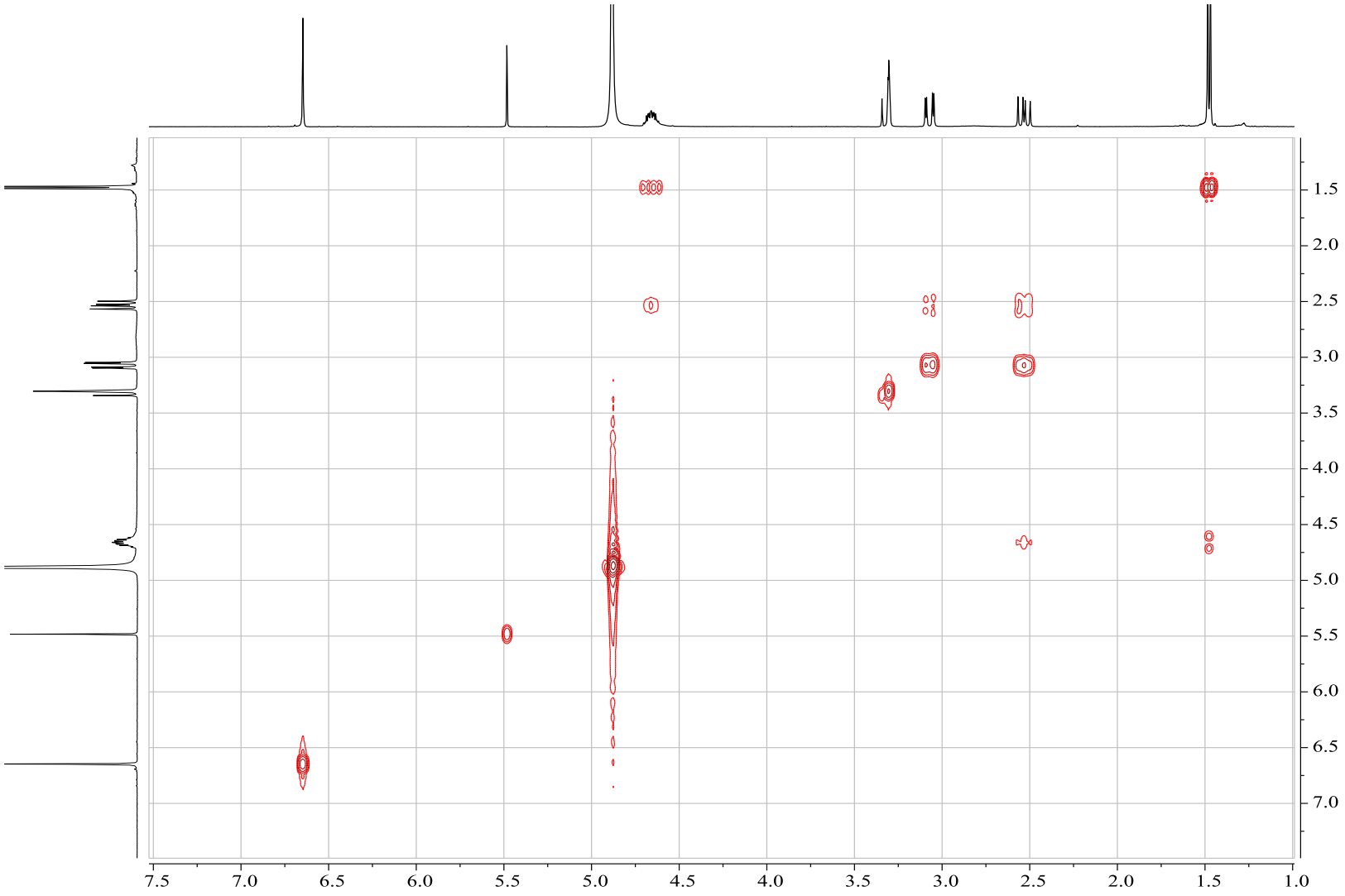

Figure S34. COSY spectrum of **4**.

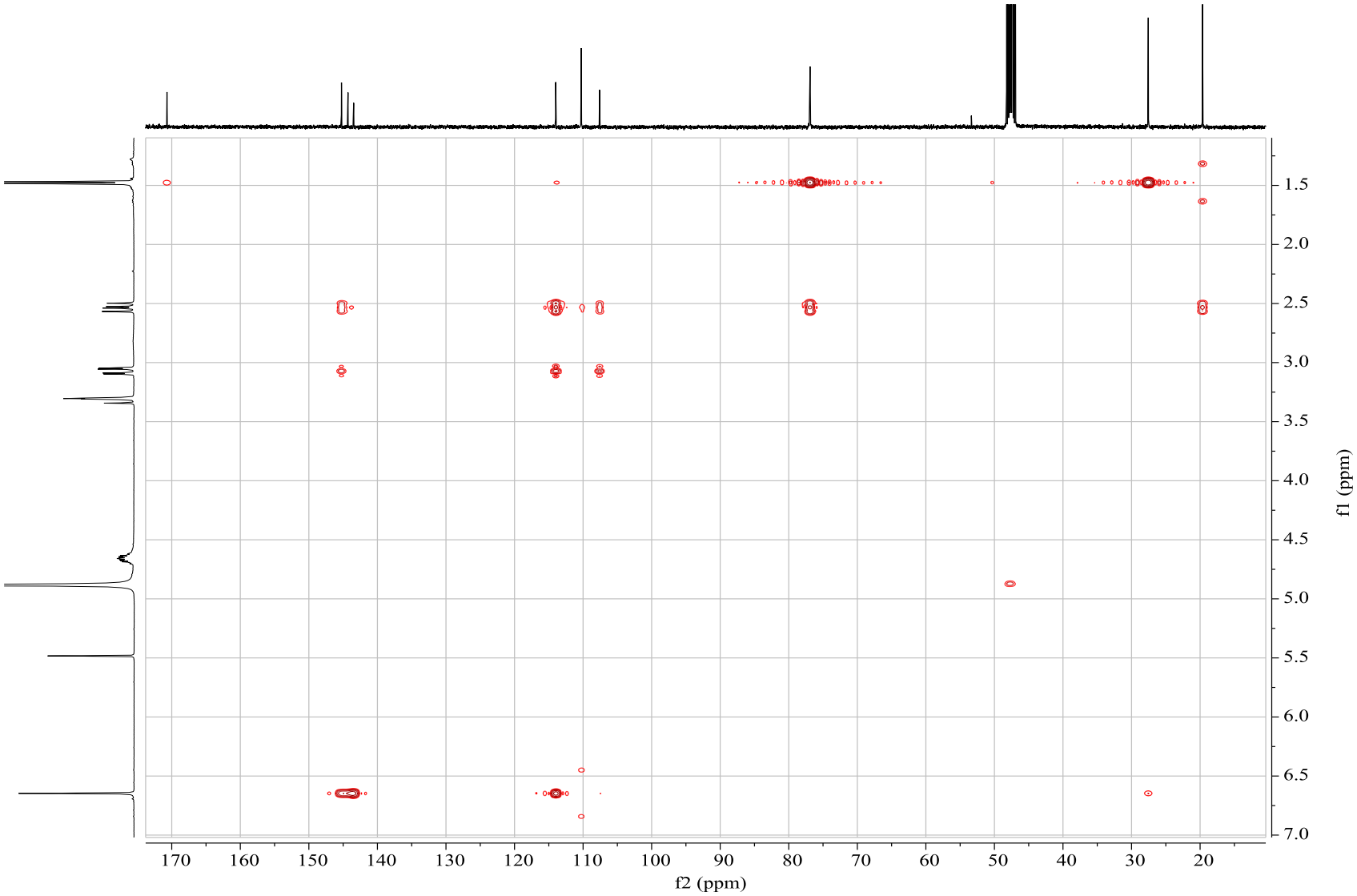

Figure S35. HMBC spectrum of **4**.

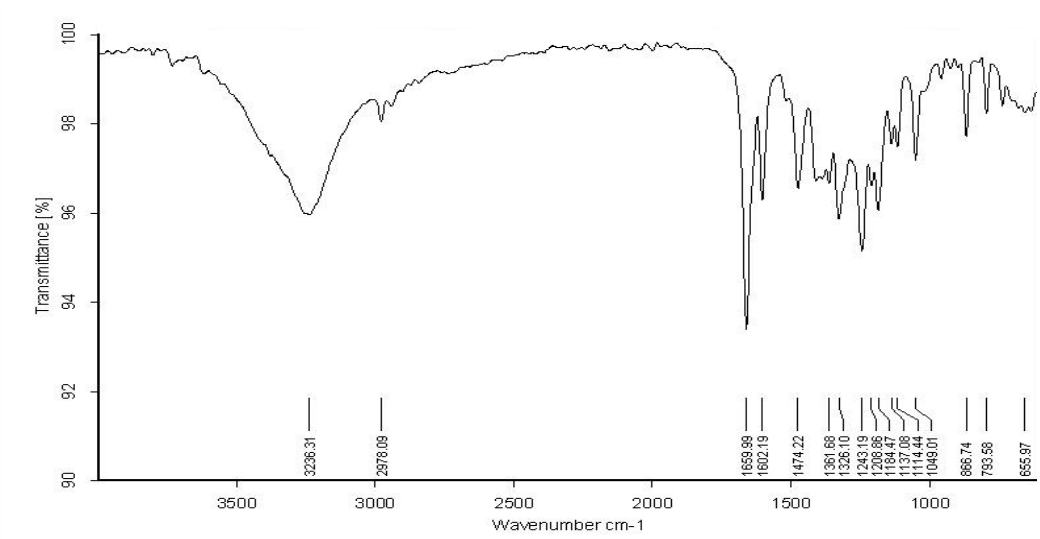

Figure S36. IR spectrum of **4**.

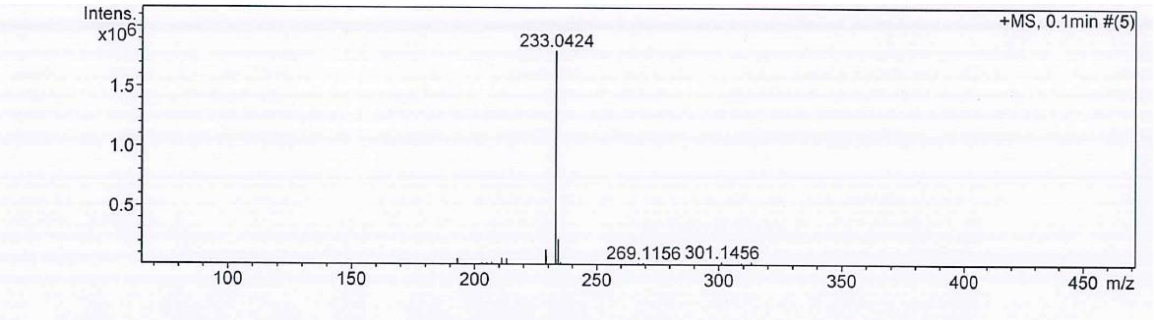

Figure S37. HR-ESI-MS of **4**.

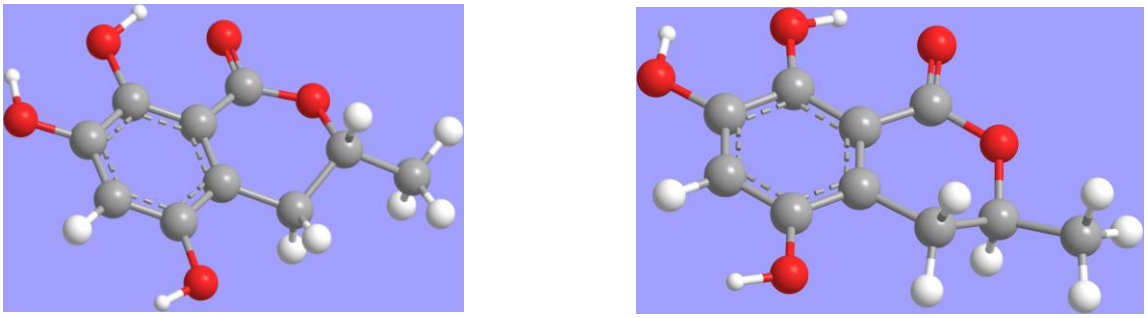

Figure S38. The global minimum energy conformers and the percentage of Boltzmann popularity of (3*R*)-**4** and (3*S*)-**4**

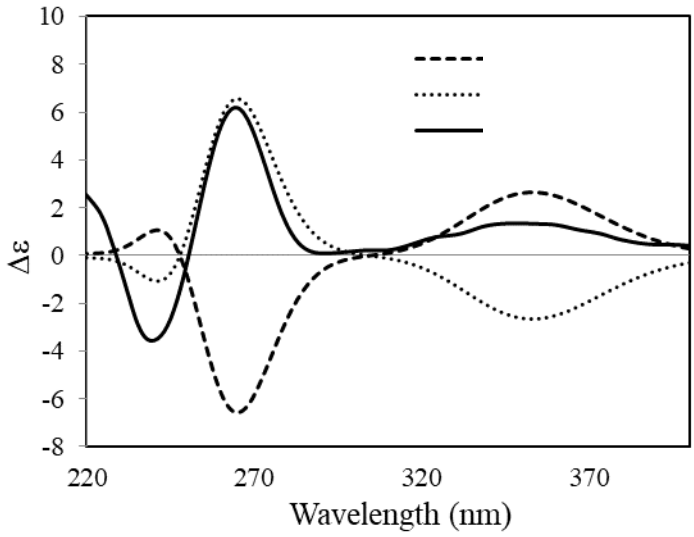

Figure S39. Comparison of calculated ECD and experimental spectra of **4**.

Table S5. The ^{1}H NMR data of **5**, mellein (Chacón-Morales et al. 2013), **6**, (*R*)-7-hydroxymellein (Liu et al. 2006), **7**, (*S*)-8-*O*-methylmellein (Kerti et al. 2007), **8**, (*R*)-5-methoxycarbonylmellein (Klaiklay et al. 2012) in $CDCl_3$.

Position	5	Mellein	6	(*R*)-7-Hydroxy-mellein	7	(*S*)-8-*O*-Methylmellein	8	(*R*)-5-Methoxycarbonyl-mellein
1								

Position	5	Mellein 6	(*R*)-7-Hydroxymellein 7	(*S*)-8-*O*-Methylmellein 8	(*R*)-5-Methoxycarbonylmellein	
2						
3	4.73 (sextet, 7.2)	4.74 (tq, 6.9, 6.3)	4.74 (q, 6.4)	4.66 (dq, 6.5, 6.5)	4.55 (m)	4.54-4.58 (m)	4.67 (m)	4.68 (m)
4	2.93 (d, 7.2)	2.93 (dm, 6.9, 1.0, 0.7)	2.88 (t, 8.0)	2.80 (d, 6.5)	2.91 (dd, 16.1, 10.6) 2.84 (dd, 16.1, 3.6)	2.89 (dd, 16.0, 10.9) 2.85 (dd, 16.0, 3.2)	3.88 (dd, 16.0, 4.0) 3.03 (dd, 16.0, 12.0)	3.88 (dd, 17.7, 3.0) 3.05 (dd, 17.7, 12.0)
4a								
5	6.89 (d, 8.4)	6.69 (dq, 7.4, 1.0)	6.62 (d, 8.0)	6.55 (d, 8.0)	6.79 (d, 7.5)	6.79 (d, 8.0)		
6	7.40 (dd, 8.4, 7.6)	7.41 (dd, 8.4, 7.4)	7.08 (d, 8.1)	7.01 (d, 8.0)	7.45 (dd, 8.5, 7.5)	7.45 (t, 8.0)	8.13 (d, 9.0)	8.13 (d, 9.0)
7	6.69 (dd, 7.6, 1.2)	6.89 (m, 8.4, 1.0, 0.7)			6.91 (d, 8.5)	6.91 (d, 8.0)	6.94 (d, 9.0)	6.94 (d, 9.0)
8								
8a								
3-CH_3	1.53 (d, 7.2)	1.53 (d, 6.3)	1.53 (d, 6.4)	1.47 (d, 6.5)	1.48 (d, 6.3)	1.48 (d, 6.3)	1.56 (d, 6.4)	1.57 (d, 6.3)
7-OCH_3								
8-OCH_3					3.94 (s)	3.95 (s)		
8-OH	11.03 (s)	11.03 (d, 0.5)	11.08 (s)				11.83 (s)	11.83 (s)
1′								
2′							3.88 (s)	3.86 (s)

Table S6. The ^{13}C NMR data of **5**, mellein (Chacón-Morales et al. 2013), **6**, (*R*)-7-hydroxymellein (Liu et al. 2006), **7**, (*S*)-8-*O*-methylmellein (Kerti et al. 2007), **8**, (*R*)-5-methoxycarbonylmellein (Klaiklay et al. 2012) in $CDCl_3$.

1	169.9	170.0	170.1	169.5	162.6	162.6	170.0	170.0
2								
3	76.1	76.2	77.1	77.0	74.0	74.1	75.6	75.6
4	34.6	34.7	33.9	34.0	36.1	36.1	32.6	32.6
4a	139.4	139.5	129.6	129.6	141.9	142.0	143.5	143.5
5	117.9	118.0	117.6	117.7	119.1	119.2	118.6	118.6
6	136.1	136.2	120.5	120.4	134.3	134.4	138.5	138.5
7	116.2	116.4	143.8	143.9	110.9	110.9	116.2	116.2
8	162.2	162.3	149.0	149.0	161.2	161.3	165.5	165.5
8a	108.3	108.4	108.1	108.2	113.7	113.9	108.9	108.9
3-CH_3	20.7	20.9	20.7	20.7	20.6	20.7	20.8	20.8
7-OCH_3								
8-OCH_3					56.1	56.2		
8-OH								
1′							166.2	166.2
2′							52.0	52.0

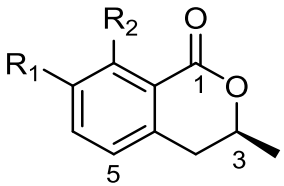

3 R_1 = OC
5 R_1 = H,
6 R_1 = OH
7 R_1 = H,

Figure S40. Structures of compounds **3** and **5-8**.

Table S7. The ^{1}H and ^{13}C NMR comparison of **9**, **10**, (3*R*,4*S*)-4-hydroxymellein (Devys et al. 1992) and (3*R*,4*R*)-4-hydroxymellein (Djoukeng et al. 2009) in $CDCl_3$.

Position	**Compound 9**		**(3*R*,4*S*)-4-Hydroxymellein**		**Compound 10**		**(3*R*,4*R*)-4-Hydroxymellein**	
	δ_H[a]	δ_C	δ_H[a]	δ_C	δ_H[a]	δ_C	δ_H[a]	δ_C
1		168.5		168.5		169.2		169.1
3	4.55-4.62 (brs)	80.0	4.59-4.63 (m)	80.0	4.67 (qd, 6.6, 2.1)	78.2	4.68 (q, 6.9)	78.1
4	4.55-4.62 (brs)	69.1	4.59-4.63 (m)	69.2	4.55 (d, 2.1)	67.2	4.55 (s)	67.2
4a		141.2		141.2		140.5		140.4
5	6.98 (d, 8.4)	116.3	7.04 (d, 8.5)	116.3	6.98 (dd, 8.5, 1.1)	118.3	7.00 (d, 7.6)	118.3
6	7.53 (t, 7.9)	136.9	7.54-7.57 (m)	136.9	7.50 (dd, 8.5, 7.2)	136.8	7.51 (t, 7.6)	136.8
7	7.02 (d, 7.4)	117.7	7.0 (d, 8.5)	117.8	6.90 (dd, 7.4, 1.1)	118.4	6.90 (d, 7.6)	118.5
8		161.9		162.0		162.0		162.1
8a		106.6		106.7		106.8		106.8
3-CH_3	1.50 (d, 4.8)	17.9	1.52 (d, 5.5)	17.9	1.55 (d, 6.6)	16.0	1.57 (d, 6.9)	16.0
8-OH	10.95 (s)		11.0 (s)		10.92 (s)		10.98 (s)	
							1.85 (brs)	

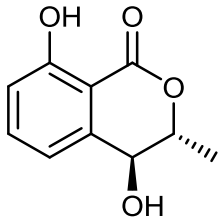

(3*R*,4*S*)-4-Hydroxymellein (**9**)

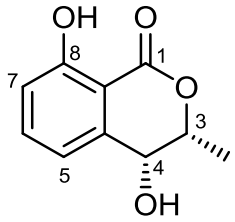

(3*R*,4*R*)-4-Hydroxymellein (**10**)

Figure S41. Structures of compounds **9** and **10**.

Table S8. The ^{1}H and ^{13}C NMR data of **11** ($CDCl_3$), **12** ($CDCl_3$), (1'*R*)-dehydropestalotin ($CDCl_3$) (Evidente et al. 2012).

Position	Compound 11		Compound 12		(l'*R*)-Dehydropestalotin
	δ_H	δ_C	δ_H	δ_C	δ_H
2		166.9		164.5	
3	5.14 (s)	90.6	5.42 (d, 2.2)	88.1	5.33 (d, 2.0)
4		173.1		171.4	
5	2.52 (t, 6.3)	27.6	6.08 (d, 2.2)	98.5	6.02 (d, 2.0)
6	4.34 (t, 6.4)	64.4		166.4	
1′			4.36 (dd, 7.6, 4.8)	70.7	4.30 (m)
2′			1.63-173 (m)	34.8	1.75 (m)
			180-188 (m)		
3′			1.28-1.43(m)	27.2	1.33 (m)
4′			1.28-1.43 (m)	22.4	1.33 (m)
5′			0.89 (t, 7.2)	13.9	0.89 (t,7.0)
4-OCH_3	3.74 (s)	55.9	3.80 (s)	55.9	3.72 (s)

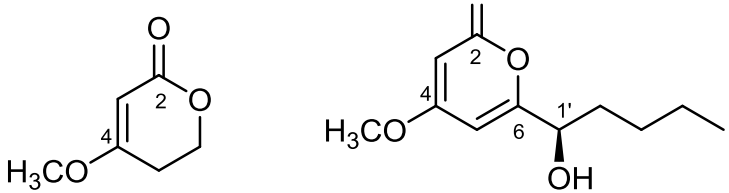

11 **12**

Figure S42. Structures of compounds **11** and **12**.

Table S9. The ^{1}H and ^{13}C NMR data of **15** (Methanol-d_4) and cytidine (DMSO-d_6) (Adam et al. 2005)

Position	Compound 15		Cytidine	
	δ_H [a]	δ_C	δ_H [a]	δ_C
2		151.0		156.9
4		164.8		166.7
5	5.70 (d, 8.1)	101.2	5.84	95.7
6	8.01 (d, 8.1)	141.3	7.79	142.8
1′	5.90 (d, 4.5)	89.2	5.99	90.1
2′	4.17 (t, 4.9)	74.3	4.25	75.1
3′	4.14 (t, 4.9)	69.9	4.15	70.6
4′	4.00 (dd, 4.5, 2.7)	84.9	4.08	85.3
5′	3.83 (dd, 12.2, 2.7)	60.8	3.88	61.9
	3.73 (dd, 12.3, 3.1)		3.76	

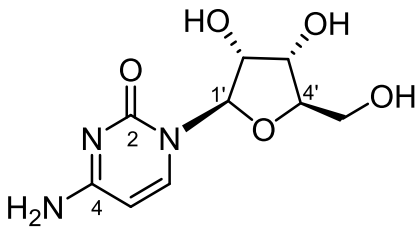

Figure S43. Structure of compound **15**.

Table S10. Physical properties of the isolated compounds

Compound	Appearance	Melting point (^{o}C)	Optical rotation
1	White amorphous solid	240-241	
2	White amorphous solid	225-226	
3	White amorphous solid	108-110	$[\alpha]_D^{26.1}$ +57 (*c* 0.6, CH_2Cl_2)
4	White amorphous solid	217-220	$[\alpha]_D^{21.6}$ +13.7 (*c* 0.1, MeOH)
5	White amorphous solid	49-50	$[\alpha]_D^{21.9}$ +17.8 (*c* = 1.0, MeOH)
6	White amorphous solid	82-84	$[\alpha]_D^{26.4}$ +53 (*c* = 1.00, CH_2Cl_2)
7	White amorphous solid		$[\alpha]_D^{21.7}$ +54 (*c* = 0.50, $CHCl_3$)
8	White amorphous solid	63-65	$[\alpha]_D^{24.8}$ -57.4 (*c* = 1.00, CH_2Cl_2)
9	White amorphous solid	124-125	$[\alpha]_D^{27}$ -21 (*c* = 0.5, MeOH)
10	White amorphous solid	71-73	$[\alpha]_D^{27}$ -18 (*c* = 0.5, MeOH)
11	White amorphous solid		
12	Yellow oil		$[\alpha]_D$ +27.3 (*c* = 0.50, MeOH)
13	White amorphous solid	144-145	
14	White amorphous solid	177-180	
15	Yellow oil		

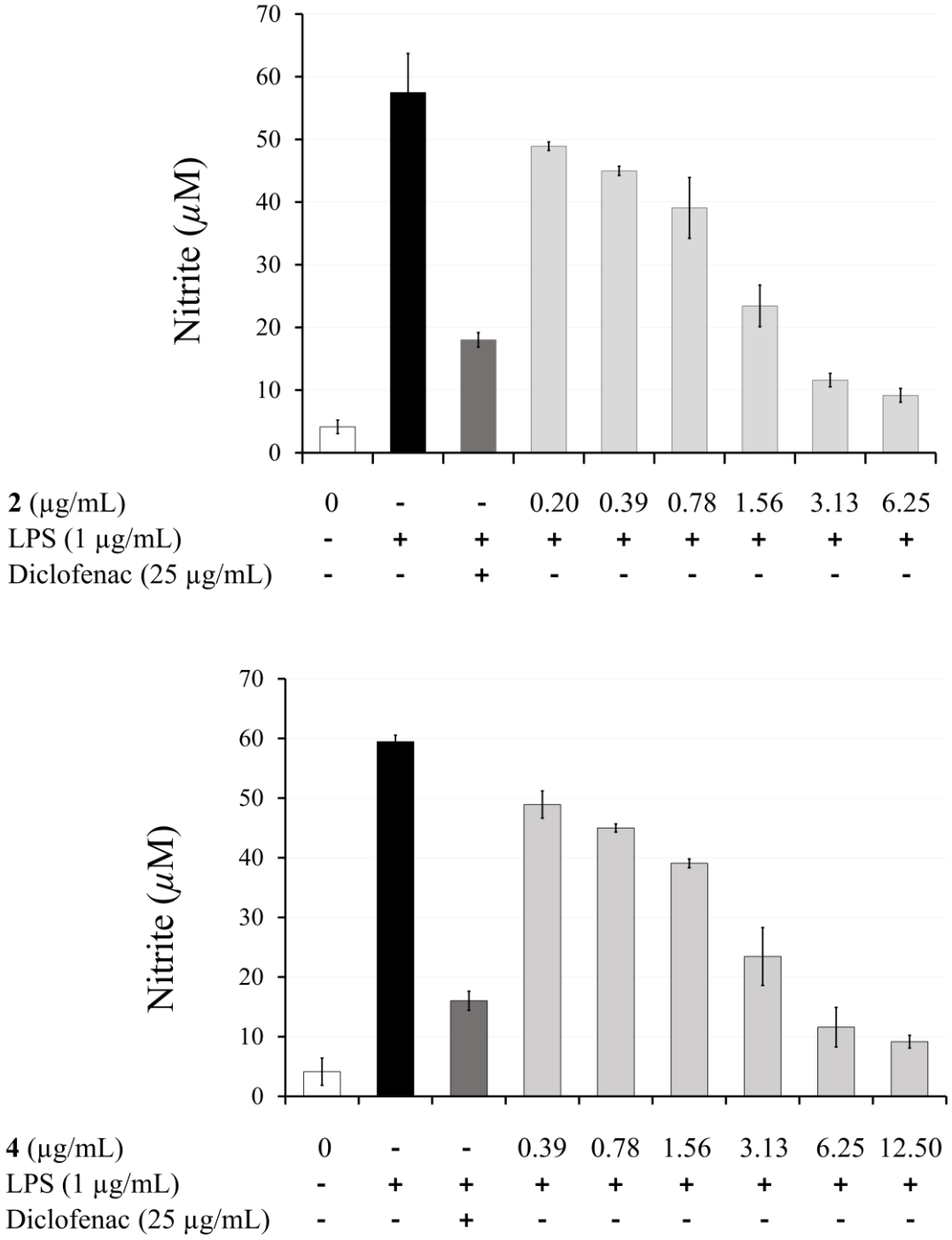

Figure S44. Inhibitory effects of **2** and **4** on nitric oxide (NO) production in LPS-activated RAW 264.7 macrophages.

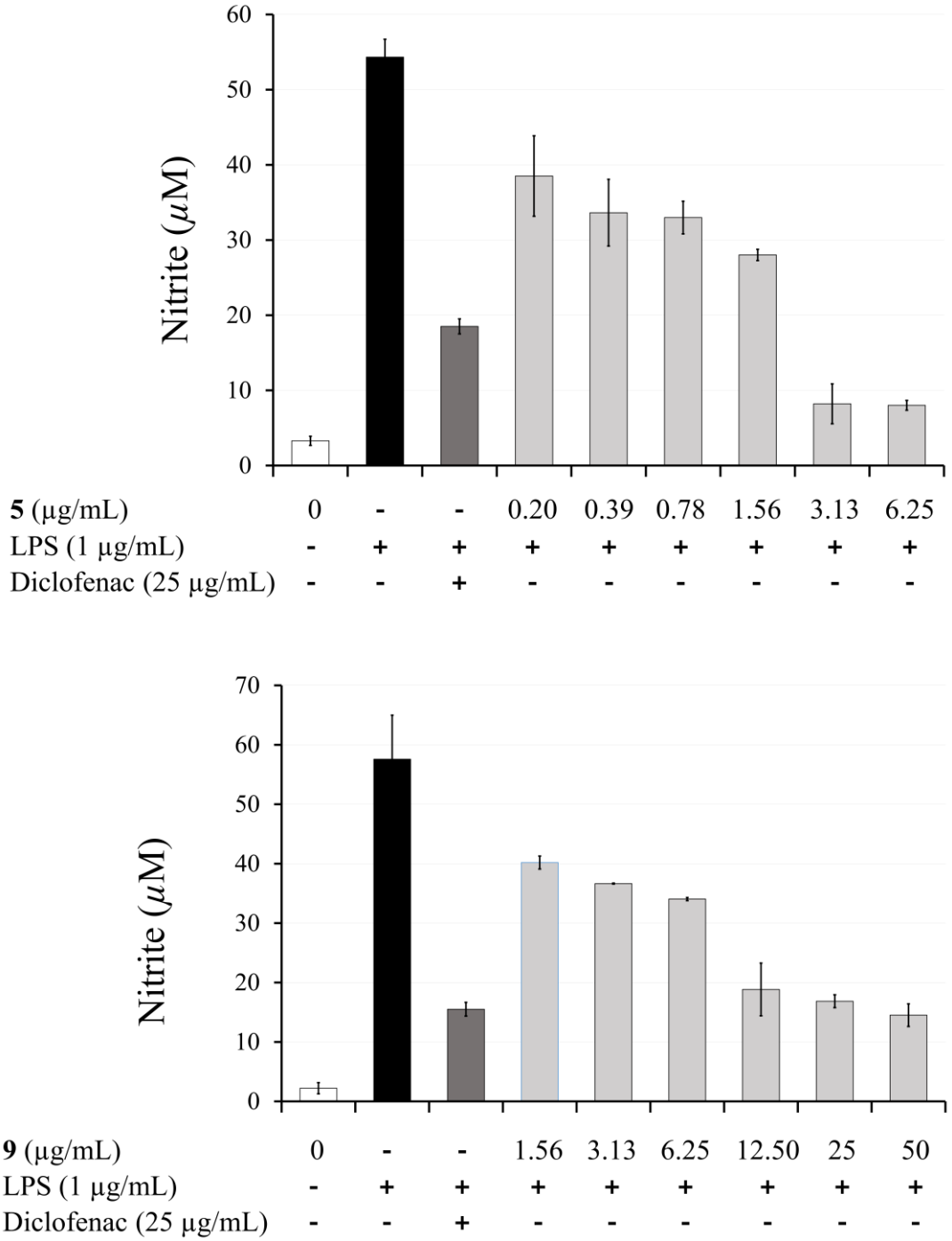

Figure S45. Inhibitory effects of **5** and **9** on nitric oxide (NO) production in LPS-activated RAW 264.7 macrophages.

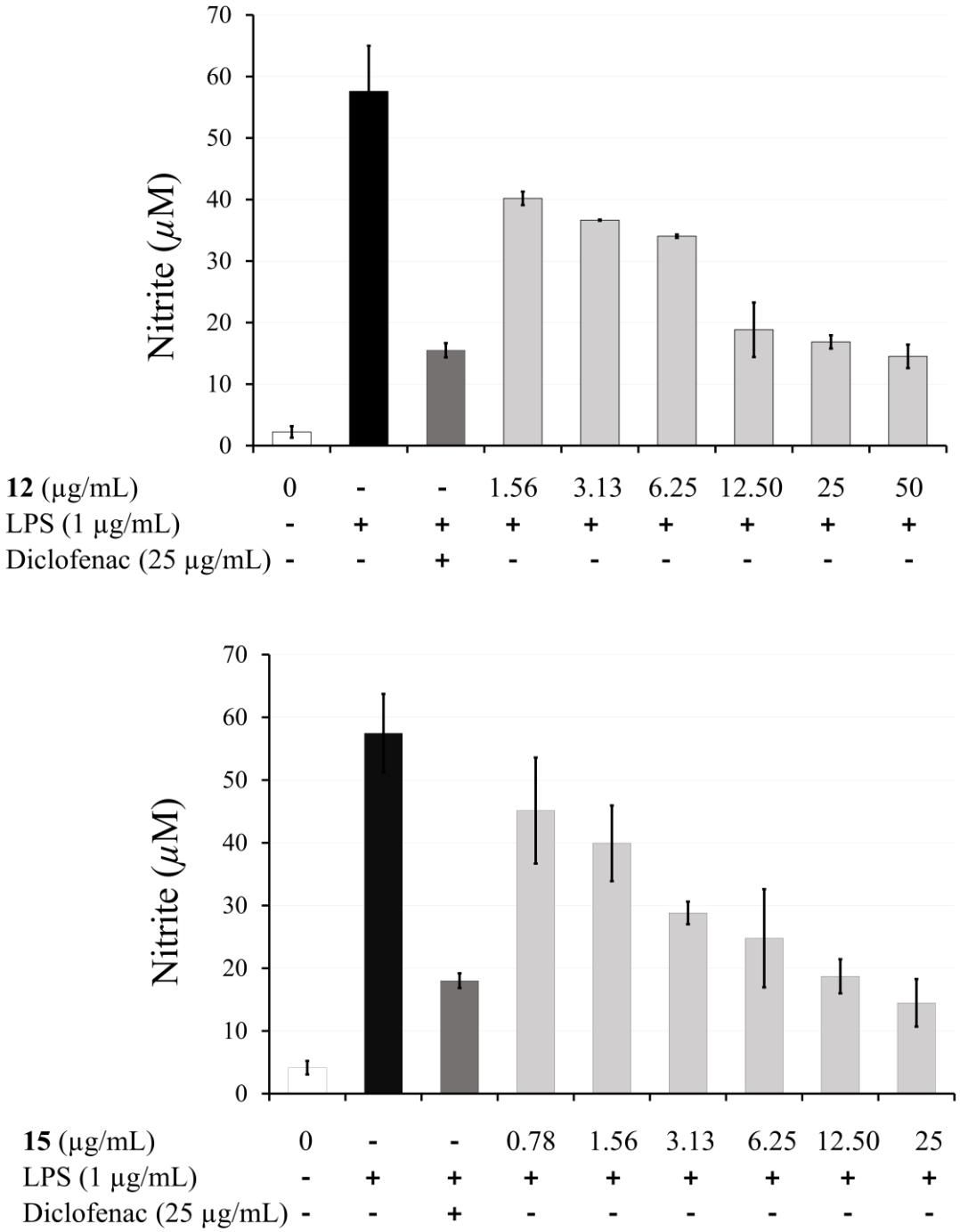

Figure S46. Inhibitory effects of **12** and **15** on nitric oxide (NO) production in LPS-activated RAW 264.7 macrophages.

References

Adam P, Gütlich M, Oschkinat H, Bacher A, Eisenreich W. 2005. Studies of the intermediary metabolism in cultured cells of the insect *Spodoptera frugiperda* using ^{13}C- or ^{15}N-labelled tracers. BMC Biochem. 6:24.

Chacón-Morales P, Amaro-Luis JM, Bahsas A. 2013. Isolation and characterization of (+)-mellein, the first isocoumarin reported in *Stevia* genus. Av en Quim. 8:145–151.

Cossi M, Rega N, Scalmani G, Barone V. 2003. Energies, structures, and electronic properties of molecules in solution with the C-PCM solvation model. J Comput Chem. 24:669–681.

Devys M, Barbier M, Bousquet J-F, Kollmann A. 1992. Isolation o f the new (-)-(3*R*,4*S*)-4-hydroxymellein from the fungus *Septoria nodorum* Berk. Zeitschrift für Naturforsch. 47:779–781.

Djoukeng JD, Polli S, Larignon P, Abou-Mansour E. 2009. Identification of phytotoxins from *Botryosphaeria obtusa*, a pathogen of black dead arm disease of grapevine. Eur J Plant Pathol. 124:303–308.

Eko A, Hiroshi N. 2014. Circular dichroism calculation for natural products. J Nat Med.:1–10.

Evidente A, Zonno MC, Andolfi A, Troise C, Cimmino A, Vurro M. 2012. Phytotoxic α-pyrones produced by *Pestalotiopsis guepinii*, the causal agent of hazelnut twig blight. J Antibiot (Tokyo). 65:203–206.

Frisch MJ, Trucks GW, Schlegel HB, Scuseria GE, Robb MA, Cheeseman JR, Scalmani G, Barone V, Mennucci B, Petersson GA, et al. 2010. Gaussian 09, revision B. 01. [place unknown]: Gaussian Inc., Wallingford CT.

Kerti G, Kurtán T, Illyés T-Z, Kövér KE, Sólyom S, Pescitelli G, Fujioka N, Berova N, Antus S. 2007. Enantioselective synthesis of 3-methylisochromans and determination of their absolute configurations by circular dichroism. European J Org Chem.:296–305.

Klaiklay S, Rukachaisirikul V, Sukpondma Y, Phongpaichit S, Buatong J, Bussaban B. 2012. Metabolites from the mangrove-derived fungus *Xylaria cubensis* PSU-MA34. Arch Pharm Res. 35:1127–1131.

Liu X, Xu F, Zhang Y, Liu L, Huang H, She Z, Lin Y, Chan W. 2006. Crystal structure of 3*S*-hydroxy-7-melleine. Chinese J Chem Phys. 19:423–427.

Yanai T, Tew DP, Handy NC. 2004. A new hybrid exchange–correlation functional using the Coulomb-attenuating method (CAM-B3LYP). Chem Phys Lett. 393:51–57.